1-1-1979

A study of the pulsar in a binary system.

Lee Allen Fowler
University of Massachusetts Amherst

A STUDY OF THE PULSAR IN A BINARY SYSTEM

A Dissertation Presented

By

LEE ALLEN FOWLER

Submitted to the Graduate School of the
University of Massachusetts in partial fulfillment
of the requirements for the degree of

DOCTOR OF PHILOSOPHY

February 1979

Astronomy

National Science Foundation
AST-77-20019

A STUDY OF THE PULSAR

IN A BINARY SYSTEM

A Dissertation Presented

By

LEE ALLEN FOWLER

Approved as to style and content by:

Joseph H. Taylor
Chairman of Committee

Eugene Tademaru
Eugene Tademaru, Member

Nicholas Z. Scoville, Member

James F. Walker, Jr.
James F. Walker, Member

F. W. Byron, Jr.
Frederick W. Byron, Jr., Head
Department of Physics
and Astronomy

ACKNOWLEDGEMENTS

This dissertation has been brought to completion only with the encouragement, assistance, and collaboration of many people. A full acknowledgement of everyone is, of course, impossible, but I should like now to mention the more important of those also involved in the work.

I would like to thank the staff of the Arecibo Observatory for many many hours of assistance during my observing runs, and for their generously provided equipment, facilities, and data reduction programs. My observations were made in collaboration with Jim Cordes, Joe Taylor, Peter McCulloch, Tim Hankins, Russ Hulse, Gordon Gullahorn, Peter Backus, and Joanna Rankin. The flux and polarimetry analysis benefitted in particular from contact with Jim Cordes. Ted Harrison, George Greenstein and David Van Blerkom were of great help in considering with me some of the observable aspects of the binary system covered in Chapter V. However, the person of prime importance throughout my graduate career has been Joe Taylor, to whom I turned with my problems and my excitement, and who was always the source of encouragement and insight.

I had the help of Steven Lord, Peter Backus, Jim Cordes and Dave Helfand for critical readings of the dissertation. And I am very appreciative of Geary Gravel for his two-fingered virtuosity with the typewriter, and for his excellent proofing and unshrinking humor.

I never had a lack of encouragement or support. To family, friends, colleagues, and especially to Carol, I thank you very much.

ABSTRACT

A STUDY OF THE PULSAR IN A BINARY SYSTEM

(February 1979)

Lee A. Fowler, B.A., Cornell University

Ph.D., University of Massachusetts

Directed by: Professor Joseph H. Taylor

For the past four years, PSR 1913+16 has been observed extensively at radio frequencies for purposes of better understanding the pulsar and the binary system of which it is a member. With the data obtained, a preliminary determination of the individual masses of the pulsar and the undetected companion is now available. It is also possible to place more stringent limits on the possible stellar type of the companion.

After a brief review of the salient characteristics of pulsars and of the binary pulsar, the data acquisition procedure at the Arecibo Observatory is discussed. The data reduction computer programs and the least squares fit method are described, by which pulse arrival times are used to produce estimates of the pulsar and orbital values and formal errors. A table of best currently available estimates is presented. The formal errors are then discussed in view of measurement uncertainties and possible systematic errors present in the arrival time data.

Flux density measurements of the radio radiation at

430 MHz and 1420 MHz are presented. These measurements show possible variation of the flux over the last few years. The dispersion measure of the pulsar is found to be 171.64 ± .01 pc cm^{-3}, and shows no significant variation with the orbital phase of the pulsar, allowing strong limits to be set on the local electron density. Pulse shapes for 430 MHz and 1420 MHz are presented. The integrated pulse profile at 430 MHz is found to be ~25% linearly polarized. An unsuccessful search for a hypothetical pulsar companion is described.

A method for determining and independently checking the individual masses of the system components is described, and preliminary calculations presented. The pulsar mass is $(.9 \pm .6)M_{\odot}$ and the companion mass is $(1.9 \pm .6)M_{\odot}$. These masses are in good agreement with the independent check available. The indications are that the system behaves dynamically as two point masses.

We also report a preliminary determination of a decrease of the orbital period of the binary system. This decrease is consistent with the interpretation that energy is being lost to the system by radiation of gravitational waves as predicted by General Relativity. A change of the 430 MHz mean pulse shape between 1977 July and 1978 June is suggestive of a relativistic precession of the pulsar's spin axis due to spin-orbit interactions in the system. The observations to date are also used to test the viability of metric

theories of gravity that have been suggested as alternatives to General Relativity.

Proposed evolutionary scenarios of the binary system are summarized and their contribution to the understanding of the companion's stellar type evaluated. Two observational tests of possible white dwarf and helium core star companions are presented, with the conclusion that these objects are becoming increasingly unlikely as possible companions. After discussion of a tentative optical detection of a faint object at the timing position of the pulsar, at variance with the weight of the findings of this dissertation, a prospectus for future observations is given. A final summary follows. All of the studies reported in this dissertation are consistent with the binary system's consisting of the observed pulsar in orbit with a roughly 1 - 2 $M_{\odot}$ companion which behaves like a point mass. Possible companions are: a slowly rotating white dwarf, a black hole, or a neutron star. The latter object is favored on evolutionary grounds.

TABLE OF CONTENTS

LIST OF TABLES

LIST OF FIGURES

C H A P T E R I

INTRODUCTION

§1. A First Look

The discovery of the first pulsar was made in late 1967 by Jocelyn Bell, a graduate student of Cambridge University astronomer Anthony Hewish (Hewish et al. 1968). Several hundred pulsars have since been discovered. Understanding of the physical processes involved in these fascinating objects has advanced considerably since initial startled speculation about alien civilizations. Pulsars are now believed to be rapidly rotating neutron stars; their characteristic regular bursts of radio radiation are interpreted as flashes from a continuous beam of intense radio emission repeatedly carried through our line of sight by the star's rotation.

There are 320 pulsars known as of 1978 July. Among these pulsars, it appears that PSR 1913+16 is the only one that is a member of a binary system. The lack of binary pulsar systems seems unusual at first, since roughly half of the stars in our galaxy are found in binary and multiple systems. The explanation is likely to be found in the evolutionary history of such systems.

The one known exception, PSR 1913+16, is the topic of my dissertation, and may well prove to be as exciting a probe into the physical universe as pulsars themselves. The importance of finding a pulsar in a binary system will be

clearer after a brief review of some of the pertinent properties of pulsars.

§2. A Brief Review of Pulsars

The single most significant characteristic of pulsars, and the key to the importance of the binary pulsar, is their highly regular pulsation rate. Pulsars have been observed with periods ranging between 33 μs and 4.3 s. With the exception of the binary pulsar, these periods are constant to about 1 part in 10^{14} per period, and most are many orders of magnitude better. The pulsed emission usually occupies only a small fraction of the pulsar period, called the duty cycle. Observed duty cycles for most pulsars are around 1% to 5%.

The source of energy for the pulsar appears to be the spin of the neutron star itself (Gold 1968). Spin down rates (or period first derivatives) have been observed for a number of pulsars, and range from an enormous 36 ns per day for the Crab nebula pulsar (PSR 0531+21) to less than 2×10^{-13} s per day, the smallest detected first derivative, for PSR 1952+29.

Each pulsar has its distinctive signature, the mean pulse shape. When individual pulses from hundreds or thousands of periods are added together and plotted as intensity against time over a period, a very stable mean (or integrated) pulse profile emerges. The stability of the profile most likely has its genesis in an extremely strong magnetic

field of approximately 10^{12} gauss (Radhakrishnan and Cooke 1969) which is rigidly anchored to the surface of the neutron star. Although large variations in individual pulses are observed, the shape of the mean pulse profile seems to be constant over many years (Helfand et al. 1975). The polarization of the integrated profiles has also been studied (Manchester et al. 1975). Many pulsars have some degree of linear polarization, with the radio signal almost completely polarized in a few cases. Circular polarization is sometimes present, usually at around 5% of the total intensity.

The structure and polarization of single pulses on millisecond and microsecond timescales are currently receiving considerable attention (Cordes and Hankins 1977), as they contain much information about the emission mechanism and pulsar magnetosphere. However, the binary pulsar is too weak for studies of single pulses with current techniques.

i) Pulsar timing.

Because many of the results of our research are based on a timing analysis of the pulsar, it is appropriate to include a brief description of information gained by timing pulse arrivals from other pulsars. The period (and period derivative when detectable) are found from the pulse repetition rate. Additionally, the arrival time depends on the location and motion of the earth and the angle between the earth and the pulsar as measured at the center of mass of

the solar system. Because the earth's orbit is about 1000 light-seconds across, an arrival time measurement accuracy of about 100 μs allows a determination of the position of the pulsar to ~0.1 arcsec in the best cases. From changes in this timing position over several years, proper motions of a few pulsars have been determined. By timing the arrival of the same pulse at different frequencies, the dispersion measure of the pulsar can be calculated (see section III-3 for details).

ii) Theoretical models.

It is now widely agreed that pulsars are highly magnetized rotating neutron stars. The high stability and shortness of period and the smallness of the duty cycle caused the eventual rejection of other suggested physical models, such as pulsating neutron stars and pulsating or rotating white dwarfs. A neutron star is an extremely condensed star containing about one solar mass in an object of about 10 km radius. The magnetic field is of order 10^{12} gauss and is rigidly locked into place by the crystalline surface formed by iron nuclei at high density and pressure (Ruderman 1972). The exact form of the magnetosphere of the pulsar has not yet been determined, and the emission mechanism whereby the intense radio emission is generated and collimated into a narrow beam is not understood (Manchester et al. 1973, Komesaroff 1970, Radhakrishnan and Cooke 1969). The most probable location of the emission region is at or near the

magnetic polar region of the neutron star. A beam of coherent radiation is emitted by energetic particles in the presence of the large magnetic and electric fields. The rotation of the pulsar (since the magnetic field can be offset from the spin axis) then causes this beam to sweep across our line of sight. The many specific models that have been proposed are reviewed in the literature cited above.

§3. The Binary Pulsar

The binary pulsar was discovered by Hulse and Taylor (1975a) during the course of a very sensitive systematic search for pulsars conducted at the Arecibo Observatory. The description of the instrumentation and search techniques used in the pulsar survey can be found in Hulse and Taylor (1975b). The pulsar was of immediate interest because it had the second shortest period yet discovered. Subsequent attempts to determine the period to an accuracy of ±1 μs were thwarted by changes in the observed period by as much as 8 μs in 5 minutes. (Compare with 36 ns per day for the Crab pulsar.) It soon became apparent that the period changes could be understood as Doppler shifts resulting from orbital motion of the pulsar around a companion object. Under this assumption, radial velocities of the pulsar were obtained over an entire orbital period, and plotted as a function of orbital phase. The velocity curve resulting from that plot has been replotted without the data points as

the heavy line in figure I-1.

The orbital elements of the system were determined in the same fashion as solving for the elements of a single line spectroscopic binary system (Aitken 1964). The orbital period is slightly less than a third of a day, and the orbit has a semimajor axis of about 1 solar radius. The orbit is very eccentric ($e \approx .617$) and the major axis of the ellipse lies nearly in the plane of the sky, the reason for the symmetry of the heavy line in figure I-1. The inclination angle between the orbital plane and the plane of the sky is indeterminate in the single line binary solution. The drawing of the system shown in figure I-2 is for $i = 90°$. The complete set of our best orbital parameters is given in Table II-3.

It was immediately obvious that the system could be an excellent testing ground for various general relativistic effects and alternative gravitational theories (Hulse and Taylor 1975a, Esposito and Harrison 1975). The extremely regular pulsar signal provides a good "clock in an orbit" and the eccentric orbit moves the pulsar in and out of the gravitational field of the companion.

The companion of the pulsar cannot be a main sequence star. The type of companion star is restricted by the size of the semimajor axis, the lack of pulsar eclipses, and the observed rate of advance of periastron (described below). Initial calculations published in the discovery paper showed

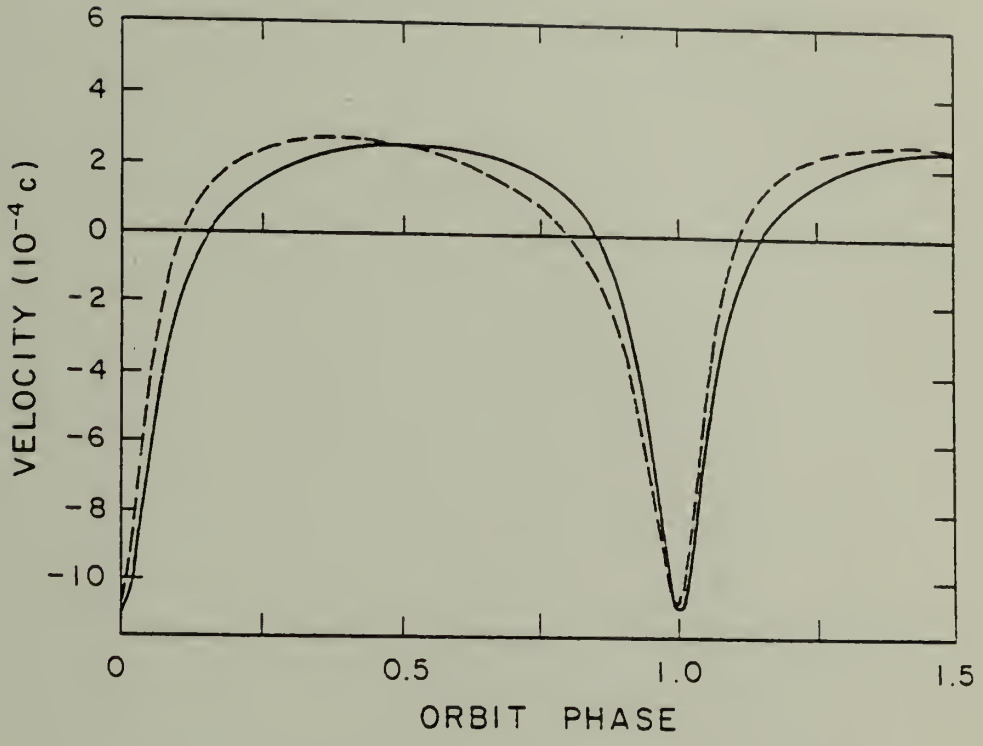

Figure I-1. The velocity curve of the pulsar as a function of orbit phase. The heavy line indicates the curve for 1974 September. The dashed line is for 1978 March. The velocity of the pulsar is about one thousandth the velocity of light near periastron.

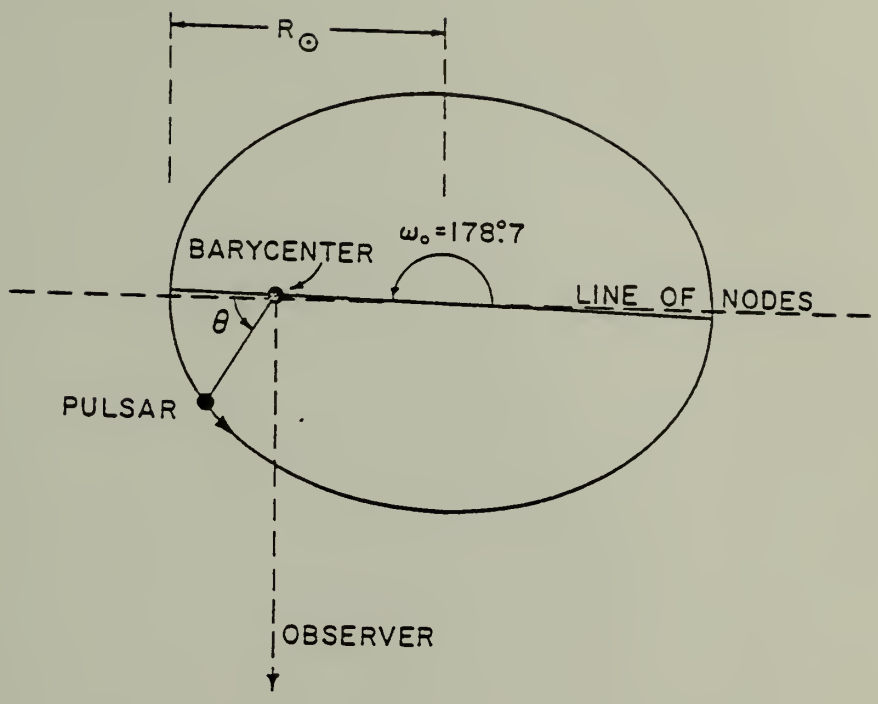

Figure I-2. The orbit of the pulsar with respect to the center of mass. For an observer in the plane of the page, the inclination angle is 90°.

that the geometrical constraints of the system all but rule out main sequence stars. Masters and Roberts (1975) subsequently have shown that the classical periastron advance from rotational and tidal distortions of a main sequence companion would be at least a thousand times larger than the observed value. Therefore the companion must be a compact object: a neutron star, black hole, helium core, or white dwarf.

In the absence of rotational or tidal distortion of the companion, the entire periastron advance will be due to General Relativity. The relativistic rate of periastron advance per orbit, $\dot{\omega}_{GR}$, for a system comprised of a pulsar of mass M_p and a companion of mass M_c is

$$\dot{\omega}_{GR} = \frac{6\pi G}{c^2} \frac{(M_p+M_c)^{2/3}}{a_1 \sin i} \frac{f_m^{1/3}}{(1-e^2)} \qquad \text{(I-1)}$$

where e is the orbital eccentricity and f_m is the mass function. The mass function can be evaluated in terms of measured quantities and Kepler's laws.

$$f_m = \frac{(M_c \sin i)^3}{(M_c+M_p)^2} = .1312\ M_\odot \qquad \text{(I-2)}$$

We then have that $\dot{\omega}_{GR}$ for the binary system (in deg yr^{-1})

$$\dot{\omega}_{GR} = 2.105 \left(\frac{M_p+M_c}{M_\odot}\right)^3 \text{deg yr}^{-1} \qquad \text{(I-3)}$$

and an advance of about 4 deg yr^{-1} was anticipated (Hulse and Taylor 1975a). Compare this value to the 43 arcsec $century^{-1}$ for the perihelion advance of Mercury, the magnitude of this

effect in the solar system. In addition, the transverse Doppler shift and gravitational redshift should be measurable. And if observations are carried on long enough, a decrease in the orbital period might be measurable. The decrease could be due to energy loss by gravitation radiation and would provide the first proof of the existence of gravitational waves.

After a year of observations, another paper was published (Taylor et al. 1976). More accurate values for the pulsar and orbital parameters were presented, including a determination of the periastron advance. (Best current value is $\dot{\omega} \approx 4.22°/\text{yr.}$) If $\dot{\omega} = \dot{\omega}_{GR}$, then the total mass of the system can be determined from (I-2).

$$M_T = M_p + M_c = 2.840\ M_\odot \qquad \text{(I-4)}$$

The dashed line in figure I-1 is the velocity curve for the binary pulsar in 1978 March. The advance of periastron has destroyed the symmetry and substantially changed the shape of the curve.

§4. Dissertation Contents

I have several reasons for writing this dissertation. The first and foremost is to report and summarize research I have been engaged in over the past three years towards fulfillment of my Ph.D. requirements. The second reason is to document extensively the data I have acquired so that it

will be of maximum use in future studies of the binary pulsar. Finally, I wish to review theoretical work to date, and describe recent improvements in the observational techniques which may lead to additional results in the near future.

The second chapter contains the documentation of the data. The first sections deal with the observing sessions and telescope systems at Arecibo Observatory, and the data reduction programs at Amherst. The final two sections present the results of the timing analysis and comment on the presence of random and systematic errors, their origins and effects on the timing results.

Chapter III concerns itself with other studies I have made of the pulsar, including flux measurements, determination of the dispersion measure, description of the mean pulse shape and the polarization of the pulsar, and the results of a search for a radio pulsar companion.

Chapter IV describes the various relativistic effects and tests the system may make possible. Current results of tests on some alternative gravitational theories are reported. I also present a discussion of additional relativistic effects that may be observable in the system when a longer time base and higher quality timing data are available.

Chapter V summarizes theoretical work on the evolutionary history of the system ending with a synopsis of what I have learned and anticipating what progress can be made in

the immediate future.

C H A P T E R I I

DATA ACQUISITION AND PROCESSING

§1. Introduction

This chapter contains a thorough discussion of the arrival time data and of its use in obtaining estimates of the pulsar parameters and binary system orbital elements. The next section is a general description of some of the requirements of binary pulsar timing. Section 3 describes the 430 MHz and 1420 MHz observing systems of the 305 m telescope at the National Astronomy and Ionosphere Center at Arecibo, P.R. The data reduction programs and the pulsar timing equation are discussed in section 4. A table of the final values of the pulsar and orbital parameters is presented in this section, however comprehensive discussion of the results is deferred to chapter IV. The final section presents an analysis of the various random and systematic errors present in the data, an estimate of their magnitude, and the degree to which they affect the results.

§2. Binary Pulsar Timing Requirements

This section is concerned with requirements that are placed on the telescope and computer data taking programs for determining accurate arrival times from PSR 1913+16. The binary pulsar is estimated from its dispersion measure

to be about 5 kpc distant. The pulsed emission is correspondingly extremely weak and the first consideration is always one of having sufficient bandwidth and long enough integration times to achieve a reasonable signal-to-noise ratio. The length of the integration has a natural upper limit of about 20 minutes, determined by the necessity of having several data samples as the pulsar moves rapidly through periastron passage. In practice, 5 minute integrations were generally used.

There is also a limit to the bandwidth that can be used. The presence of free electrons in the interstellar medium causes the pulse to arrive successively later at lower frequencies. The time lag between the undelayed signal and the actual arrival is proportional to the dispersion measure and the inverse square of the observing frequency. For the binary pulsar, the pulse lags by about 1/3 of the period across a 1 MHz bandwidth at 430 MHz. The pulse smeared by such a large amount is clearly unsuitable for pulse timing, and the technique that has evolved to alleviate this problem involves chopping up the incoming bandwidth into many discrete channels with a multichannel filter-bank. The signal output from each channel is then delayed by an interval appropriate for its center frequency and the dispersion measure of the pulsar. The outputs can then be summed to achieve the full bandwidth of the filter-bank, yet suffer only the dispersive smearing present across

an individual filter. The 32 × 20 kHz filter-bank receiver used at 430 MHz caused 340 μs of dispersive smearing.

The radio spectrum of the pulsar is such that the flux of the pulsar at 1420 MHz is only 1/6 of the flux received at 430 MHz. For this reason, all of the early timing data was taken at 430 MHz. However, with the acquisition of a 2 × 32 × 250 kHz filter-bank in 1977 July, it became possible to use the 1420 MHz telescope system. The poorer telescope gain is offset by the better system temperature at the higher frequency. The 16 MHz bandwidth of signal compensates for the decreased pulsar flux, and the dispersive smearing across one 250 kHz channel at 1420 MHz is only 130 μs. This compares to 340 μs of smearing across the 20 kHz filters used at 430 MHz. Timing data taken at the higher frequency is of superior quality and measurement error is estimated to be no more than about 60 μs for a single 5 minute integration arrival time.

The timing data were recorded using one of two different computer programs at Arecibo. In the first case, the digitized output from the telescope was sampled under computer control and written onto magnetic tape without additional processing. The magnetic tapes were then brought to Amherst for subsequent processing. In the terminology of this dissertation, these data were collected with fast-sampling techniques. The second case is referred to as on-line folding. The digitized signal was sampled in a fashion similar to the

fast-sampling case. The resulting samples are then summed into a 1024 word array in such a way that the pulse phase is maintained and an average profile is produced as the data are collected. On-line folding requires an accurate knowledge of the pulsar period at the time of observing; errors introduced by poor periods cannot be removed later. The fast-sampling scheme is attractive in that the data can be refolded as improved pulsar periods become available. However, the magnetic tape consumption and the off-line data reduction processing pose problems of their own.

In all observing setups, the final signal was smoothed by an RC time constant just before digitizing, sampling and recording on magnetic tape. The amount of smoothing used depended on several factors. Large time constants improve the signal-to-noise ratio of the signal; however, if good time resolution is desired, too much smoothing can destroy information. Also, the intervals between samples should be less than or comparable to the smoothing time constant. Under-sampling, the case when the sampling interval is larger than the RC smoothing time constant, is ill advised, as information is once again being discarded. Over-sampling is not as serious; the redundant information being recorded can be discarded at a later time. The polarimetry data and some of the 430 MHz data were rather drastically over-sampled owing to the inflexibility of an Arecibo observing program. Otherwise, sampling rates were appropriate for the amount of

smoothing and dispersive smearing present in the data.

§3. Data Acquisition

i) The 430 MHz Observation System.

The initial discovery and almost all of the observations through 1976 December were made at 430 MHz. The actual 430 MHz system changed very little over the 4 years of use, and the description is appropriate for all the 430 MHz observations with only minor changes.

All observations were made with the 96 foot dual circular polarization line feed. The signal from the line feed undergoes initial amplification at the base of the feed, and then is mixed down to 30 MHz intermediate frequency (IF) and sent to the receiver room in the control building. Figure II-1 is a brief block diagram of the 430 MHz system as used in 1977 July. The parameters describing the 430 MHz system are listed in Table II-1.

ii) The 1420 MHz System.

Upon the completion of a 2 × 32 × 250 kHz filter-bank, the standard timing observing frequency was shifted to 1420 MHz. The increase in bandwidth (2 polarizations each 8 MHz *vs.* 1 polarization at .64 MHz) offset the decrease in the intrinsic pulsar flux density (.6 mJy at 1420 MHz as opposed to 4 mJy at 430 MHz). The expected improvement in arrival times was realized. Measurement uncertainty for arrival times taken in 1978 March-April was 60 μs, an improvement

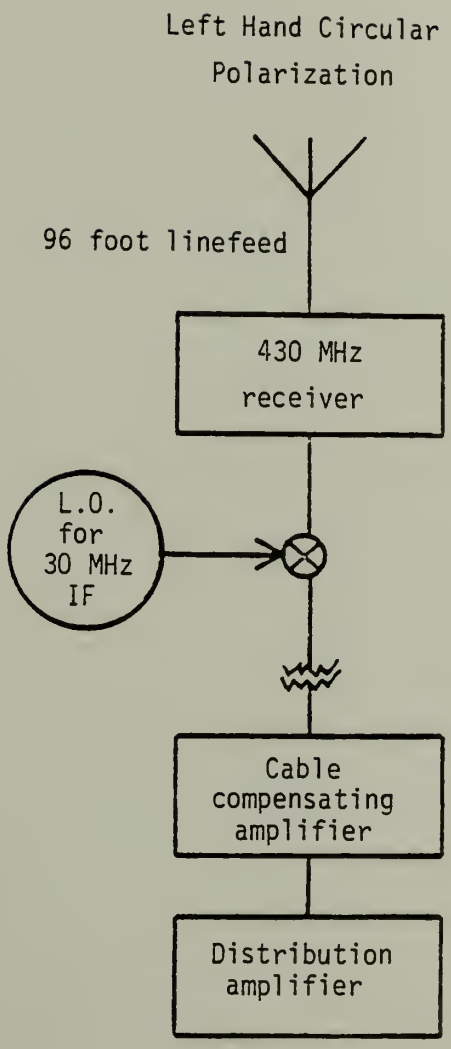

Figure II-1. Block diagram of the 430 MHz system at Arecibo Observatory.

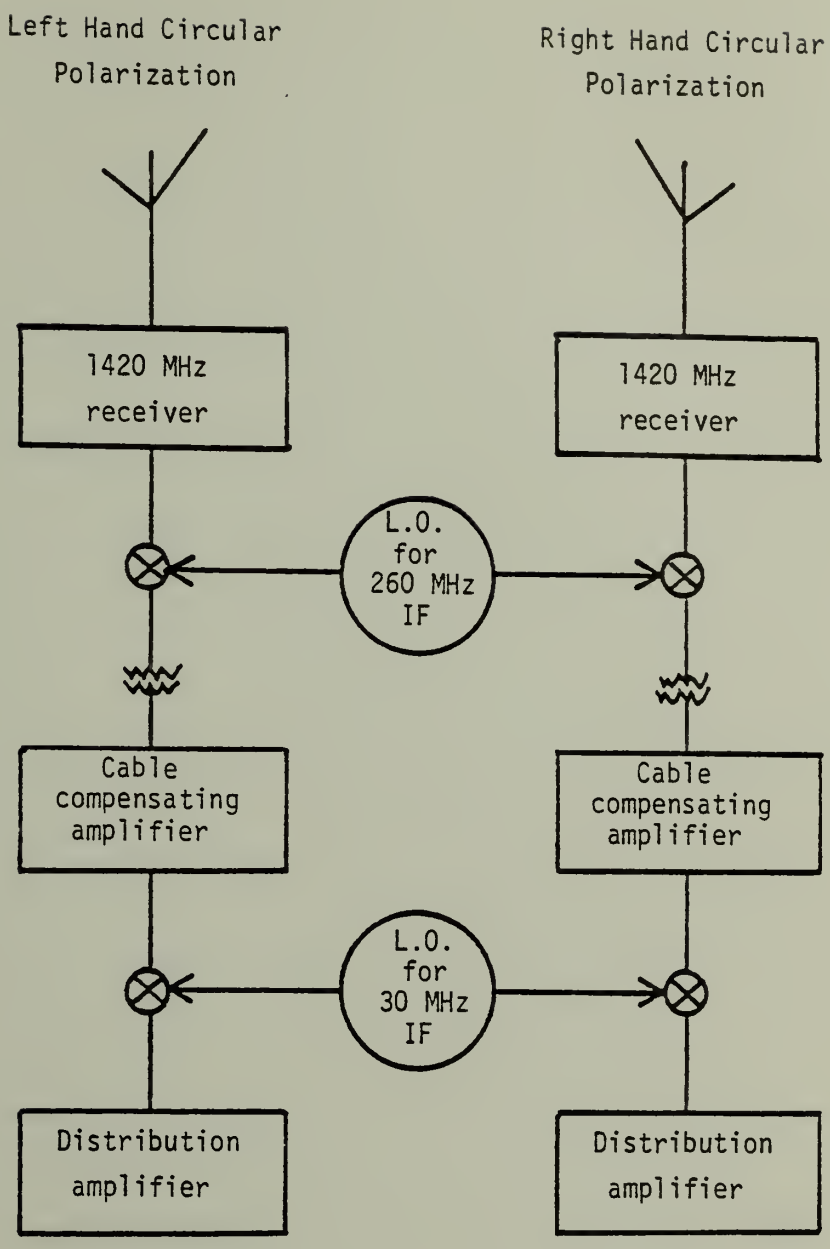

Figure II-2. Block diagram of the 1420 MHz system at Arecibo Observatory.

Table II-1. Technical information on the 430 MHz and 1420 MHz receivers and feeds at Arecibo Observatory.

Frequency (MHz)	Feed Type	Polarization	Sensitivity [2.] °K/f.u.	3 db Beamwidth (arcmin)	Receiver/ Amplifier Type	Sys. Temp. [3.] (°K)	3 db Bandwidth (MHz)
430	96' line	dual circ.	19.7	9.0	paramp	180°	10
1420	40' line	dual circ.	8.0	3.3	paramp	67°	40

Note 1. Data taken from Technical Data Sheet #2 of "The Users Manual for the Arecibo Observatory," National Astronomy and Ionosphere Center, Cornell University, Ithaca, New York

Note 2. Sensitivity at zenith. Actual sensitivity shows zenith angle dependence.

Note 3. 430 MHz system temperature includes 75°K of sky due to galactic background emission. System temperature values are taken at zenith for 1420 MHz. There is some zenith angle dependence.

of better than a factor of 3 over the 430 MHz observations.

All 1420 MHz observations made use of the 40 foot line feed. Both circularly polarized signals from the feed are mixed down to 260 MHz and sent to the control room. There, the signals are downconverted to a final intermediate frequency (IF) of 30 MHz. Figure II-2 is a block diagram of the 1420 MHz telescope system. The specifics for the 1420 MHz are also listed in Table II-1.

iii) 430 MHz Data Taking Setup.

There were a few modifications made in the 430 MHz data taking setup. The setup used in 1977 July is described below, and values of the RC smoothing time constant and sampling rates used for other observing sessions can be found in Table II-2.

The data acquisition system consisted of a 32 × 20 kHz filter-bank receiver and a digital dedispersing device (Boriakoff 1973). The left hand circular polarization (LHCP) signal was introduced to the filter-bank and the 32 channels of detected outputs sent to the dedisperser. The clock rate of the dedisperser was adjusted such that longer delays introduced in successively higher frequency channels exactly compensated for the dispersive delays due to the interstellar medium. The 32 channels were then summed, reconverted to an analog signal, and smoothed by a .1 ms RC time constant.

The signal was then redigitized and sampled by the ob-

Table II-2. Details of binary timing observations.

Date of observations	Number of points	Acquisition method	Time constant (μs)	Observing frequency (MHz)	Final rms uncertainty (μs)	Fraction of total weight in fit	
1974 Sept.-1975 Jan.	524	fast-sample	5000	430	220	0.053	
1975 May	79	on-line	660	430	300	0.010	1,4
-	83	on-line	660	430	1000	0.001	2,5
1976 Dec.	35	on-line	660	430	200	0.004	3,5
1976 Nov.-1976 Dec.	78	fast-sample	660	430	125	0.023	
1977 July-	28	on-line	100	1420	80	0.026	4
1977 Aug.	20	on-line	340	430	170	0.013	
1977 Dec.	23	on-line	100	1420	70	0.059	4
1978 March-1978 April	157	fast-sample	100	1420	40	0.639	
1978 June	42	Swept L.O.	43	430	60	0.171	6

1. 32 × 20 kHz filter-bank.
2. 250 kHz single channel filter.
3. 25 × 100 kHz FCRAO filter-bank.
4. Timing data with $V_{psr} < 0$ km s^{-1} not included.
5. Timing data with $V_{psr} < 50$ km s^{-1} not included.
6. 3 days of near periastron data taken by Taylor, McCulloch, and Weisberg (1978).

servatory's CDC 3300 computer. A 1024 point average pulse profile was accumulated every 5 minutes. These averages, as well as the start time of the integration interval, were recorded on magnetic tape and brought to Amherst for additional processing. For some observing sessions, the raw data was written directly onto tape and the signal averaging was completed in Amherst. A block diagram of the data taking setup is presented in Figure II-3.

iv) 1420 MHz Data Taking Setup.

The 1420 MHz data taking setup was similar in most respects to the 430 MHz setup. However, both circular polarizations could be used. The 64 channel filter-bank was used in the 2 × 32 mode, and each pair of frequency channels were summed after detection, so that the input to the dedispersing device was again 32 channels. After dedispersion, the channels were summed and smoothed by a .1 ms RC time constant. The signal was digitized and sampled by the observatory computer as before. The block diagram is shown in Figure II-4.

v) The Swept L.O. System.

The final 31 timing points were acquired with a new data taking system. The Swept L.O. system uses pre-detection dispersion removal and should reduce measurement error to below that obtainable at 430 MHz or 1420 MHz with the present setup (McCulloch, Taylor, and Weisberg 1978). The

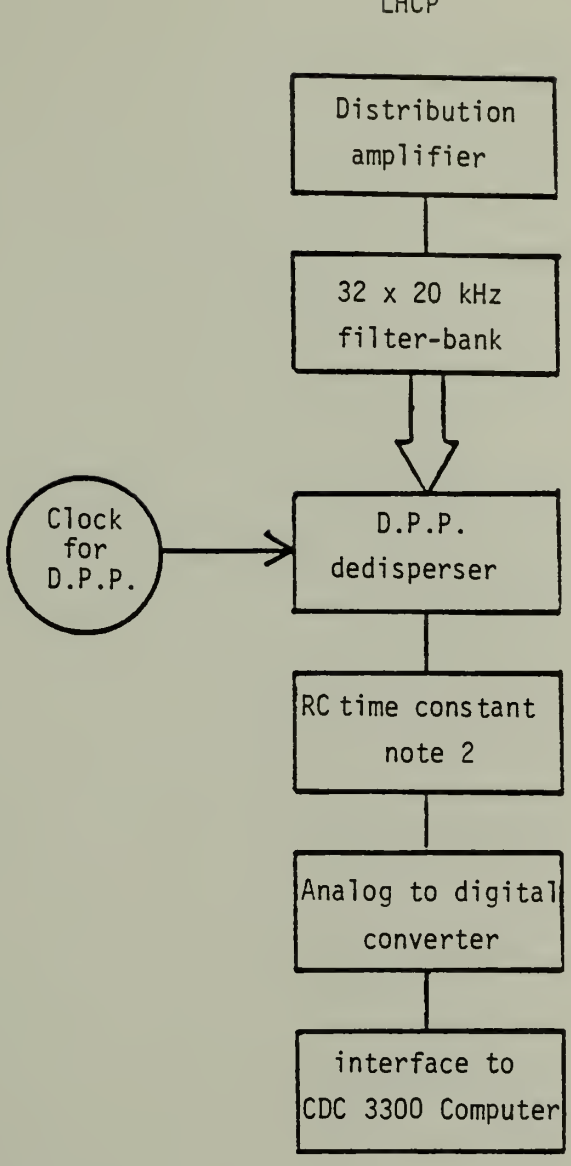

Figure II-3. The 430 MHz data taking setup.[1]

note 1. Except see Hulse and Taylor (1974) for Hulse data.

note 2. See Table II-2 for time constant values.

Figure II-4. Block diagram of the 1420 MHz data taking setup.

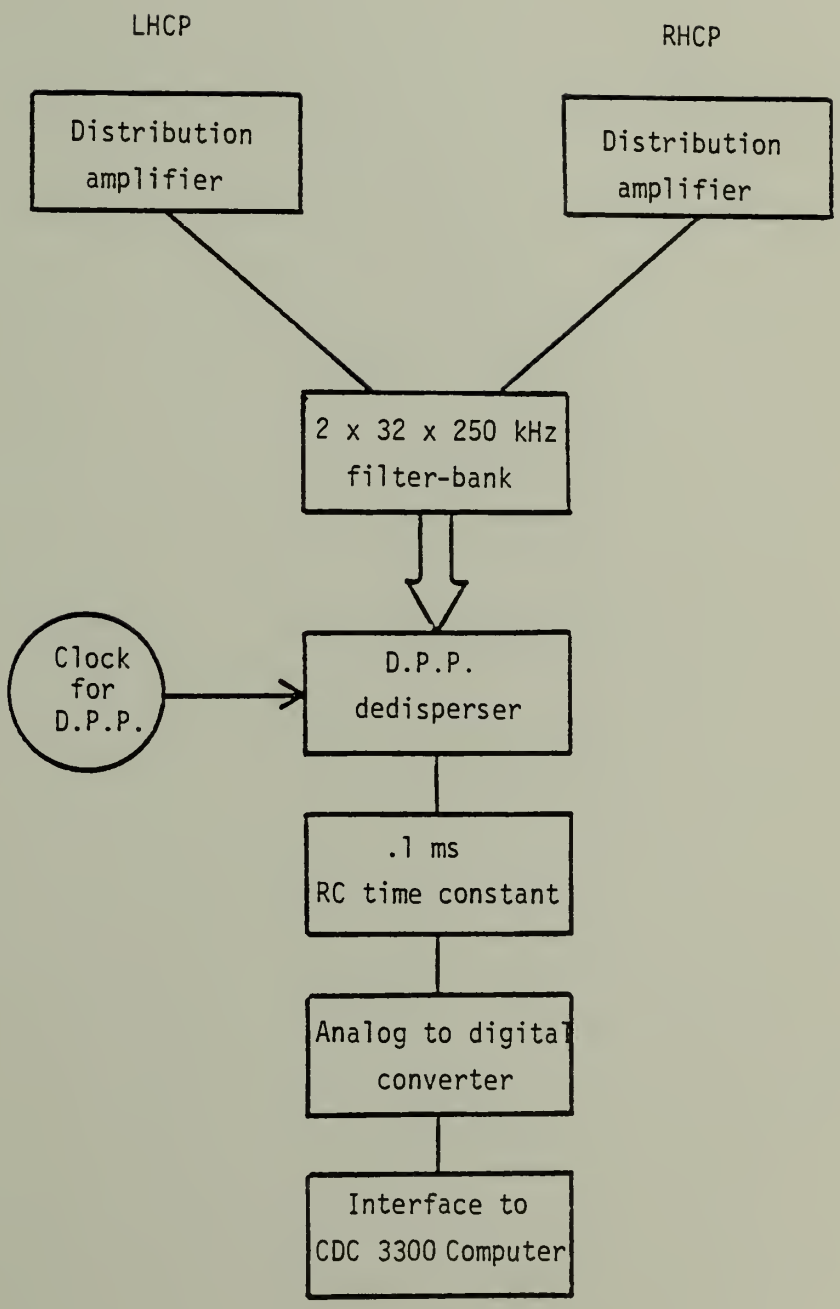
LHCP
RHCP
Distribution amplifier
Distribution amplifier
2 x 32 x 250 kHz filter-bank
Clock for D.P.P.
D.P.P. dedisperser
.1 ms RC time constant
Analog to digital converter
Interface to CDC 3300 Computer

data were taken at 430 MHz. The new system is described in the last chapter.

§4. Data Reduction

The scheme used to reduce the data is depicted in Figure II-5. The number of different reducing programs was kept to a minimum. Eventually only 2 major programs were used in the calculation of pulse arrival times. The treatment of the data was kept as uniform as possible from run to run.

i) Description of the Folding Program.

The fast-sampled data from Arecibo had to be folded modulo the appropriate pulsar period in order to build up the 5 minute average profiles used to calculate arrival times. Thus, accurate pulsar periods were needed over the time the data were taken. The folding periods were calculated directly from the least-squares fit program.

ii) Calculation of Arrival Times.

The average profiles were then processed to determine the pulse arrival times. The time of phase zero for the profile is known, having been recorded on the data tape to a nominal accuracy of 1 μs. The time to the center of the pulse is determined by fitting the 5 minute average pulse with a standard profile formed by summing in phase many 5 minute averages. In the fit, the baseline, scale, and shift

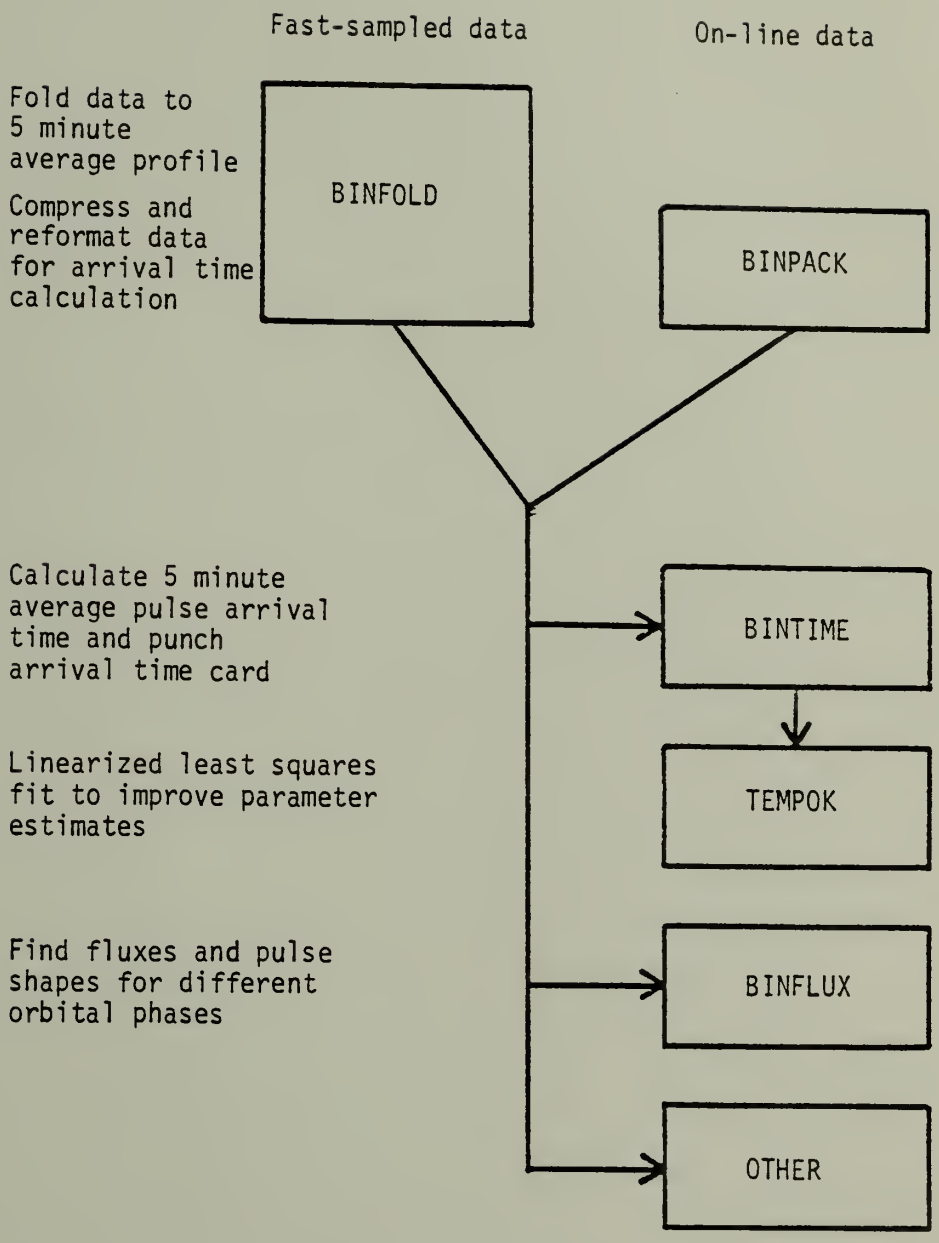

Figure II-5. The data reduction sequence.

of the standard profile relative to the 5 minute average is determined. The values determined for the three parameters are those that minimize the sum of the squared difference between the standard profile and the 5 minute average. This procedure automatically weighs the fit of the standard profile to the average by the steepest parts of the profiles because a small change in the baseline, scaling, or shift of the standard profile leads to an increase in the sum of the squared difference dominated by contributions from these sharp rise or fall times within the pulse. The pulse shape of PSR 1913+16 has a rise time of only a few hundred microseconds and is therefore excellent for timing purposes. Since the accurate shifts necessary to align the profiles are then available, a new standard profile could be created, and the process repeated until the best arrival times possible are obtained.

iii) The Least Squares Fit Program.

An understanding of the least squares fit routine is critical to the understanding of the complex timing analysis of the binary pulsar. Much judgment must be exercised and testing performed before accepting as "real" the estimates of parameters and errors made by the program. The following is a description of the program in brief and then a discussion of the timing equation for a pulsar in a binary system.

The input to the fitting routines consists of a series of arrival time cards, each one containing the measured

pulse arrival time and other required information such as the observing frequency. These arrival times (in Coordinated Universal Time as measured by the observatory clock) are then converted to solar system barycentric arrival times. The light travel time from the earth to the barycenter and the relativistic clock correction are determined from the earth's position. Next, the arrival time is corrected for the effects of dispersive delay. First the Doppler shift due to the earth's motion is removed from the observing frequency to obtain the true frequency observed at rest with respect to the dispersive medium. The dispersion measure is then used to calculate the delay experienced by the pulse against a pulse at infinite frequency which experiences no delay. The barycentric arrival time is corrected by this delay so that arrival times of different frequencies can be compared.

Next, residuals are calculated. The current best guess values of the pulsar and orbital parameters are used to predict an expected arrival time for each observed arrival time. The residuals (observed - calculated) are nonzero because of innaccuracies in the input values, measurement errors associated with the arrival times, and possible clock errors. The residuals are then weighted by a factor proportional to the inverse square of the estimated measurement uncertainty, generally taken as the rms internal scatter of the timing data in a given observing run. The internal

scatter is an indication of the amount of measurement uncertainty present in the data, and the amount of information gained from the data is maximized by the weighting scheme used. Using a least squares fit to the residuals, corrections to the input values are calculated and new best guess values found. These new values can be used as input values for additional iterations if necessary. The final values, along with their associated uncertainty estimates, constitute the output of the least squares fit routine. An important check of several aspects of the arrival time analysis was performed. A version of the least squares fit routine was written to predict arrival times from the initial estimates. These arrival times could then be fitted with the least squares fit routine as a self consistency check. Even in the presence of erroneous initial estimates of the parameters and as much as 1 ms of added zero mean gaussian noise, the least squares fit recovered the initial estimates to within the formal errors (as determined by the added noise). This self consistency was important as a check on the arrival times used in calculating the on-line folding periods and as a demonstration of the fitting routine's ability to recover the pulsar and orbital parameters in the presence of innaccurate initial guesses and measurement noise. The generated arrival times with added noise could also be used to predict the magnitude of formal errors in fitted parameters that should be present for the various

observing sessions given their differing amounts of measurement error.

iv) The Timing Equation.

The rotational frequency $\nu(t)$ of the pulsar at the neutron star surface can be expressed as a Taylor series expansion about some initial time $t = 0$.

$$\nu(t) = \nu_0 + \dot{\nu} t + \ddot{\nu} t^2 + O\left(\frac{d^3\nu}{dt^3}\right) \qquad \text{(II-1)}$$

where ν_0 is the rotational frequency at time $t = 0$. $\dot{\nu}$ and $\ddot{\nu}$ are the first and second time derivatives of the frequency, and are related to the period time derivatives as follows:

$$\dot{P} = \frac{-\dot{\nu}}{\nu^2} \qquad \ddot{P} = \frac{-\ddot{\nu}}{\nu^2} + \frac{2\dot{\nu}^2}{\nu^3} \qquad \text{(II-2)}$$

Higher order derivatives of ν are discarded. The $\ddot{\nu}$ term for PSR 1913+16 is too small for detection, and can likewise be ignored in the expansion.

Eq. (II-1) is true at the surface of the pulsar. For other pulsars, the equation also holds true at the barycenter of the solar system, if P and $\dot{P}$ are redefined slightly to take into account the relative motion and acceleration of the pulsar, and t is now defined as the arrival time of the pulse at the barycenter, adjusted to infinite frequency. For PSR 1913+16, the situation is vastly more complicated. The location of the pulsar in its orbit around the companion can introduce delays of ~±2 seconds due to light travel time across the orbit, some four or five orders of magnitude larger than

typical measurement uncertainty of ~100 μs. The gravitational redshift and transverse Doppler effects introduce cumulative delays of 5 to 10 ms. (The terms are discussed more fully in chapter IV.) Also included in the arrival time equation are the effects of ~20 μs to 100 μs amplitude due to small non-Keplerian distortions of the orbit and gravitational propagation delay as predicted by General Relativity. The overall cycle of delays in arrival times is shown in Figure II-6. The heavy line is appropriate for delays at the time of discovery; the dashed line shows the effect of the advance of periastron on the system. Needless to say, the interaction of the final pulsar and orbital parameters that go into the arrival time equation is quite complex, and a brief description of the full timing equation is given in Appendix I. Additional information and more detailed derivations can be found in Manchester and Taylor (1977), Blandford and Teukolsky (1976, hereafter referred to as B & T), and Epstein (1977). The notation used here follows that of Epstein.

The arrival time equation is of the form

$$N = N(t, \xi_i) \qquad \text{(II-3)}$$

where t is the barycentric arrival time of the Nth pulse, and ξ_i are parameters to be fitted. Using best guess values for the ξ_i's gives rise to a residual R(t) for each arrival time. For small residuals, errors in the ξ_i's, one can use a linearized form

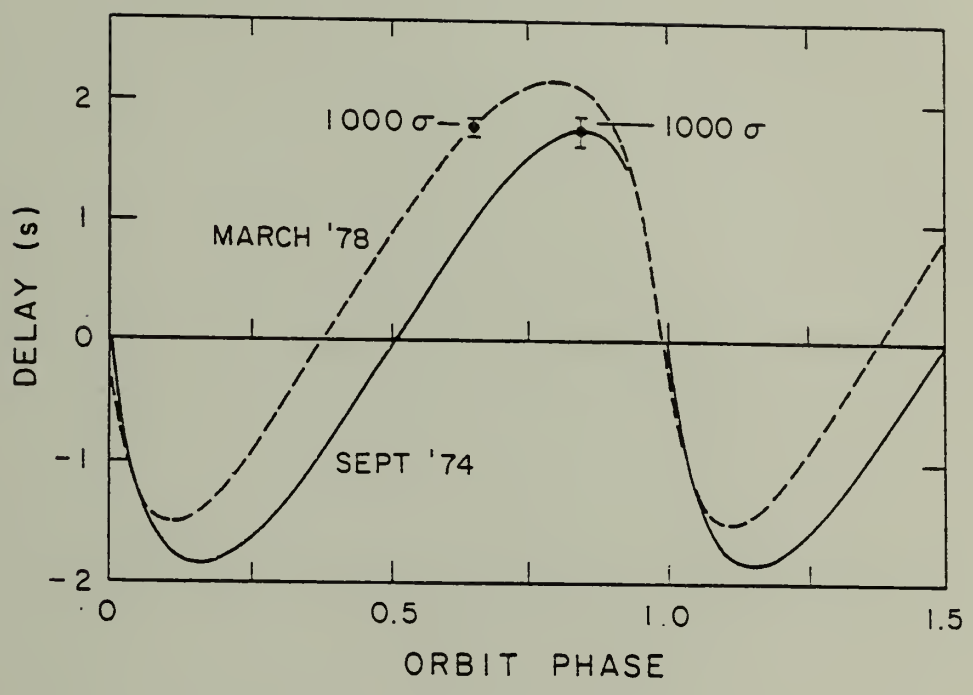

Figure II-6. Pulse arrival time delay curves for the pulsar. The heavy line indicates 1974 September, the dashed line 1978 March. The indicated data points bear error bars 1000 times the measurement uncertainties of actual data taken at those times. The time delay across the entire orbit is about 4 seconds.

$$R(t) \approx \frac{1}{\left(\frac{\partial N}{\partial t}\right)} \sum_i \frac{\partial N}{\partial \xi_i} \delta \xi_i \qquad \text{(II-4)}$$

For the simple expansion of (II-1), N(t) is obtained by integrating $\nu(t)\big|_0^t$ so that (dropping $O(\ddot{\nu})$)

$$N(t) = N_0 + \nu t + \tfrac{1}{2}\dot{\nu} t^2$$

and

$$R(t) = \frac{\delta N_0}{\nu} - t\,\frac{\delta \nu}{\nu} - t^2 \frac{\delta \dot{\nu}}{\nu} \qquad \text{(II-5)}$$

The corrections $\delta \xi_i$ are obtained by solving the set of simultaneous linear equations of II-4. At the same time, a formal error can be calculated to estimate the precision of each of the values of the parameters, given the statistical errors of the data set and their goodness of fit to the arrival time equation. Table II-3 gives a list of the final best fit values obtained by analyzing the data described above. Discussion of the values is deferred to chapter IV. Figure II-7 is a plot of timing residuals remaining after the fit that produced the parameter estimates of table II-3.

§5. Error Analysis

The value of an observational or experimental result lies as much in the confidence and trust that can be placed in the result as it does in the result itself. For this reason, the determination of the various errors likely to be present in the data and their effect on the calculation of numerical values are of considerable interest. This

Table II-3. Values of pulsar and orbital properties as determined by the least squares fit method.

Measured Parameter		
		Astrometric and pulsar "clock" effects
Right ascension	$\alpha(1950)$	$19^h\ 13^m\ 12^s.473 \pm 0.001$
Declination	$\delta(1950)$	$16°\ 01'\ 08''.24 \pm 0''.03$
Period	P (s)	0.0590299952713 ± 5
Derivative of P	$\dot{P}$ (s s^{-1})	$(8.585 \pm 0.010) \times 10^{-18}$
		Classical orbit effects
Projected semi-major axis	$x \equiv a_1 \sin i$ (s)	2.345 ± 0.004
Orbital eccentricity	e	0.617153 ± 0.000016
Binary period	P_b (s)	27906.98163 ± 0.00006
Longitude of periastron	ω (deg)	178.866 ± 0.002
Time of periastron passage	T_o (JD)	$2{,}442{,}321.433207 \pm 1$

Measured Parameter		
		Relativistic orbit effects
Rate of advance of periastron	$\dot{\omega}$ (deg yr^{-1})	4.221 ± 0.006
Second-order Doppler	γ (s)	0.0069 ± 0.003
Orbital inclination	sin i	$0.53 \begin{smallmatrix} + .4 \\ - .1 \end{smallmatrix}$
Derivative of P_b	$\dot{P}_b$ ($s\ s^{-1}$)	-2.0 ± 1.0
		Other possible effects
Derivative of x	$\dot{x}$ ($s\ s^{-1}$)	$(-1.1 \pm 1.2) \times 10^{-12}$
Derivative of e	$\dot{e}$ (s^{-1})	$(-0.39 \pm 0.15) \times 10^{-12}$
RMS residual	σ (μs)	100
Data span	t (yr)	3.7

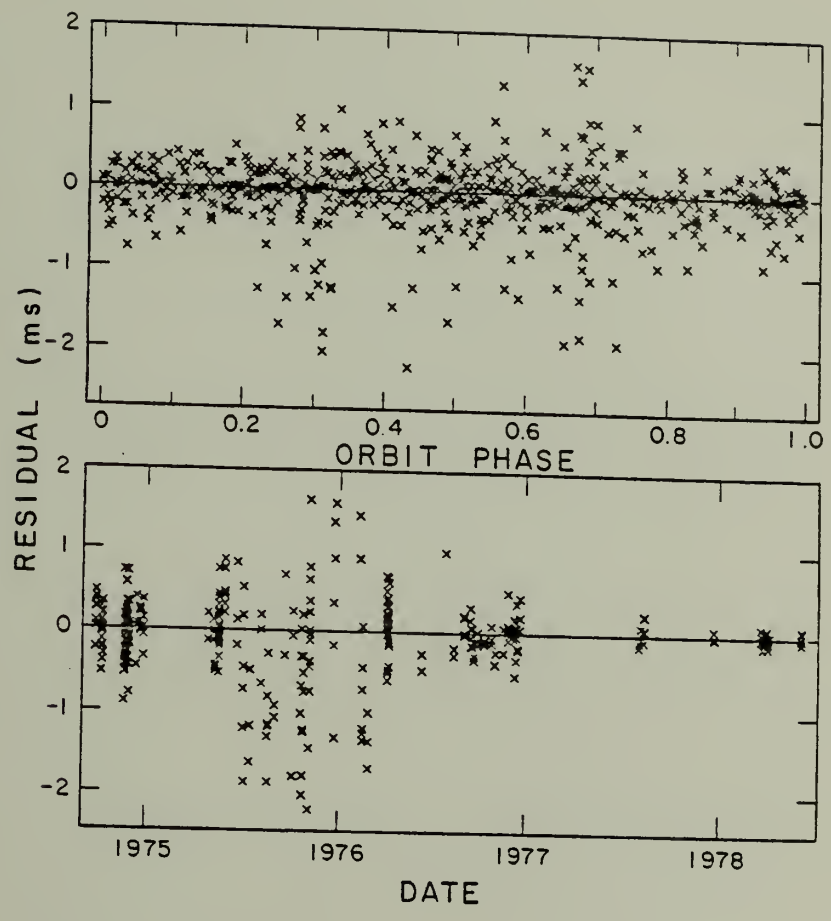

Figure II-7. Timing residuals plotted against orbit phase (upper) and date of observation (lower).

final section of chapter II will attempt to identify various errors that are likely to be important in the timing analysis, and discuss the confidence which can be lent to the final derived values and formal errors of the fit parameters presented in Table II-3 of the last section. The first treatment concerns itself with uncertainties and errors associated with determining an arrival time from a 5 minute average. The second is a discussion of the effects of systematic errors in the data, followed by a discussion of possible effects of intrinsic pulsar timing noise. Finally, each parameter in Table II-3 is discussed, and the validity of the quoted formal error established.

i) Measurement Error.

Of all the errors that may be present in the data, random measurement error is the most innocuous and its effects best understood. The measurement error referred to is the uncertainty in determining the exact arrival time of a pulse. There are several contributions to the uncertainty. The presence of galactic background noise and receiver noise contributes small random fluctuations to the 5 minute average profiles and thereby introduces an error in the calculated arrival time. The amount of noise can be made arbitrarily small in any one profile by increasing the integration interval. The same end is achieved by using several smaller intervals, and several serious problems avoided. The noise behaves like zero mean gaussian noise

with a time constant equal to the combined smoothing time constants through the radiometer system.

In addition, a small amount of more-or-less random measurement error could be introduced by variations in the pulse shape itself. Pulse-to-pulse shapes can vary tremendously, and hundreds or thousands of pulses must be summed to produce a stable mean pulse profile. Helfand et al. (1975) have determined that a sum of many thousands of pulses is required only in the presence of mode switching. Approximately 5000 pulses are accumulated to form the 5 minute average, so in all cases except severe mode switching, for which there is no evidence, these pulse-to-pulse fluctuations should contribute little to the measurement error.

Additional non-random measurement errors should be small. The clock time recorded at the start of each 5 minute average is accurate to 1 μs. At a fixed frequency, errors caused by variations in the signal travel time through the data acquisition systems are small (again of order 1 μs), though problems were encountered whenever the observing frequency was changed.

The effect of measurement uncertainty on the calculation of the formal values and determination of the formal errors is well understood. The least squares analysis employs a linearized equation for the fit, so that zero mean gaussian noise should not introduce any systematic biases

to the values. This supposition was tested in the self consistency check described in section 4 of this chapter. In the absence of systematic biases and timing noise, the final rms residual for each observational run is an indication of the measurement error for the run. The measurement error varied from 900 μs for the Gullahorn data to less than 60 μs for data taken after 1977 December.

ii) Systematic Errors.

By far the most serious errors to contend with in the timing analysis are systematic errors. The most important source of systematic errors is the use of inaccurate periods in folding the data. Arrival times derived from data folded with inaccurate periods contain systematic errors which produce a set of "corrections" to the initial estimates that can differ by many times the formal error from the actual values, and perpetuate the inaccuracies. The influence of bad periods has been overcome by use of long time baselines, by repeated refolding of fast-sampled data, and by monitoring the "drift" in phase in successive 5 minute averages. This drift is caused by accumulated phase lead or lag of successive average pulse profiles owing to a difference between the assumed and actual pulsar period. If the predicted pulse periods are exactly correct, the pulse will be frozen at a specific phase in the pulse profile. The lack of drift is the only way of knowing that the fitted parameters have no extraneous bias introduced by systematic

effects.

The long time baseline is effective in reducing the systematic errors for those parameters which are periodic, i.e. P and P_b, the pulsar period and orbital period respectively. To some extent, the errors may reappear in the time derivatives of these parameters, however refolding the fast-sampled data corrects this error, as the more accurate values of P and P_b produced give more accurate values of their derivatives.

Repeated refolding of the fast-sampled data improves the accuracy in general, because the systematic error induced in the folded data is smaller than that present in the periods used for folding. Finally, when the induced systematic error drops to the size of the sampling interval, the arrival time is no longer biased by period inaccuracies. As an example, the 1977 December profiles were observed to drift by as much as 30 sampling intervals in 5 minutes. As these data were folded on-line and cannot be refolded, the badly drifted arrival times have been discarded. In contrast, the worst drift in 1978 March - April was 30 μs in 5 minutes, or about one-third of a sampling interval. The Swept L.O. system in 1978 June manifested drifts of no more than a tenth of the smaller 43 μs sampling intervals used. The Swept L.O. data and the 1978 March - April data provided the necessary baseline with which the 1976 November - December data could be refolded. Then the time baseline was long enough that accurate periods were available for the Hulse data of late

1974 - early 1975. The current parameters should now be good enough that future on-line folding may be used without fear of biasing the arrival times with inaccurate periods.

iii) Timing Noise.

Another possible source of systematic bias to the fitted parameters or misleading formal errors in the timing analysis is timing noise intrinsic to the source. Timing noise is present in some pulsars (possibly all, with some at a level below present measurement errors). It was first extensively discussed by Boynton et al. (1972) and Groth (1975) vis-a-vis the timing of the Crab pulsar. Timing noise reveals itself as a quasi-sinusoidal curve remaining in the residuals after a fit to the data with a low order polynomial. Successive fits to the data with higher order polynomials result in a decrease in the "wavelength" of the residual fluctuations with the addition of a half "wavelength" being added for each higher order term. It was soon realized that the process was intrinsic to the pulsar. The quasi-sinusoid remaining in the residuals was the result of high frequency components of the noise spectrum. The low frequency components had in fact been absorbed by the fit and were present in the fitted values as systematic errors.

The possibility that there might be timing noise in the binary pulsar has been viewed with considerable apprehension (Discovery Paper, B & T). Timing noise cannot

ultimately prevent the establishment of the intrinsic values of the pulsar and orbital parameters. However, in the face of a large component of timing noise, it could take much longer than current expectations to determine accurate and trustworthy values for subtle effects. The equation predicting arrival times for the binary pulsar is not a simple polynomial as is the case for other pulsars, and if timing noise is in fact present, the fit to the timing data will absorb many spectral components of the noise. Also, the data were taken in typically 14 day segments separated by 2 to 9 months. Timing noise could be important on a day-to-day basis, or only important for different observing sessions. We have investigated the possibility that the data may be contaminated by timing noise at either timescale.

Timing noise is shown to be unimportant on observing session-to-session timescales by the following argument. The pulsar and orbital parameters were consistent. Each addition of data from a new observing run led to a decrease of the final rms value and and smaller formal errors. The new parameter estimates were always within the formal errors established by previous fits. If timing noise were significant, the parameters would not be predictable and would vary greatly from fit to fit as different components of the noise spectrum are absorbed.

A different approach was used to test data within a single observing run for the presence of timing noise. The

1978 March - April data was chosen for the test because of its low rms residual and large number of arrival times. In this test, the presence of timing noise would be detected as an excess of the final rms residual and of the individual formal errors over those values appropriate for 60 μs measurement error. Estimates of the final rms residual and the individual formal errors were made by dividing up the 1978 March - April data into 4 fifty-point individual subsets, each sampling an entire range of orbital phases. The 4 subsets were then processed by the least squares fit routine to determine the best parameter estimates and formal errors for each subset. The estimates of the final rms residual and formal errors appropriate for 60 μs of zero mean gaussian measurement error made use of generated data. The data were created having pulsar and orbital parameter estimates identical to the best fit estimates of the real 1978 March - April data. The data set had the same orbital sampling and total number of points as a 1978 March - April subset. The generated subset was then processed 25 times with 60 μs of gaussian noise added. From the 25 outputs, estimates of rms residual, parameter values and formal errors appropriate for 60 μs of gaussian noise were obtained. These estimates were compared to the actual values computed in the first stage. The rms residuals were comparable, and the actual formal errors were comparable or less than those predicted by the 25 realizations. Though this test cannot preclude entirely the possi-

bility of timing noise in the data, it can nonetheless be said that the formal errors are consistent with the presence of measurement error only in the data.

iv) Observing Run Offsets.

Because of frequent changes in the observing setup and data reduction that accompanied the increase in accuracy over the 4 years of observations, each observing run requires a small arbitrary offset in the nominal start time to account for slight differences in phase of the first point. These slight steps are the result of different standard profiles used in the arrival time determination, small frequency dependent delays through the dedisperser, different delays associated with the three or four time constants that have been used, and other small variations. These offsets are included as fit parameters in the least squares fit. They cannot be exactly determined, and their error contributes to the general error of the fit in the same manner as the other parameters. In the final fit, the offsets were determined to an accuracy of about 100 μs. The existence of offsets in the data is unfortunate: they contribute to the uncertainty of the final parameter estimates. Tests with generated data have indicated that the offsets do not introduce systematic errors into the values of the other fitted parameters.

v) Reliability of Values and Error Estimates.

The values and formal errors in Table II-3 are those computed in the best fit to all the data with the least

squares fit program. In the presence of possible systematic effects detailed in ii), additional commentary is necessary in cases where the formal errors may underestimate the actual uncertainty in the derived values. In these cases, the errors are determined from the actual excursion of the final values as systematically biased data is given more or less weight in the fit.

Pulsar Position

The right ascension α and the declination δ of the pulsar are very well established for purposes of timing and of searching for the pulsar or companion at radio and other frequencies. Most of the position information is contained in the Hulse data and the Gullahorn data. The systematic errors can interact with the position fit if the orbital period is not sampled completely within an interval short compared to a year. If biased periastron data comes in clumps many months apart, as is the case for the Gullahorn data, the non-random residuals from the biased periods can be absorbed in part by the position fit. The actual error should be no greater than two or three times the error quoted in Table II-3.

Period and Period Derivative

The pulsar has been observed without loss in period count over an interval of nearly 2×10^9 pulsar periods. A naive calculation indicates that the mean measurement uncertainty of 100 μs should allow determination of the period

to approximately 5 parts in 10^{14}. In fact, the actual uncertainty is almost 3 orders of magnitude larger, an increase not explained by either the arbitrary offsets between the different observing sessions or the uncertainty of $\dot{P}$. The reason for the discrepancy is that the exact value of the un-Doppler-shifted period depends on the orbital elements of the system, and the uncertainty in these elements is much larger. The several-times-formal error discrepancies between the present values and those published recently (Fowler et al.) result from biased data near periastron present in the 1977 July - August and 1977 December data, which has since been removed. It is possible that smaller shifts may occur in future fits as better values of the orbital elements are determined. An actual uncertainty of one or two times the formal error is anticipated. A similar argument pertains to the same increase for the formal error of $\dot{P}$.

Note that the period is more than sufficiently well determined for use in on-line folding routines. The period is known to 12 decimal places, and the uncertainty in $\dot{P}$ over 5 years contributes an uncertainty of about the same magnitude. For a five minute average, an accuracy of 9 decimal places is more than adequate.

$a_1 \sin i$

The projected semimajor axis is the least certain of all the orbital elements. The formal error is 3 parts in

10^4. The reason for the large error is the near degeneracy of the coefficient in the fit for $a_1 \sin i$ and γ (described below) over a short time span. In the course of several decades, the two parameters will separate completely. For the present, the fractional uncertainty in γ (and therefore in the still closely coupled $a_1 \sin i$) is nearly 1000 times the errors of the other orbital elements.

Even this rather large formal error is an underestimate of the actual uncertainty. The value of γ is not well known and any major changes in γ would result in large changes in $a_1 \sin i$. From experimental fits with different assumed values of γ, the uncertainty is found to be nearly three times as large as the quoted formal error.

It is important to note that for the purposes of the acquisition of data, the actual value of $a_1 \sin i$ is not important but the combination of $a_1 \sin i$ and γ is. Considered together, the two are known to 5 parts in 10^6. This accuracy is similar to the accuracies of the other orbital elements, and is more than sufficient to predict unbiased periods for on-line folding of timing data.

e

The eccentricity of the system is very well established, and probably doesn't vary by more than the formal error would indicate. The value is in excellent agreement with the value in Taylor *et al*. (1976) and within the errors of that published in Fowler *et al*. (1978). The marginally high eccentricity quoted in the latter paper was influenced by

the inclusion of biased periastron data in the fit.

T_0

The Julian Date of a periastron passage is also well established. The quoted error corresponds to a determination of the time of periastron to 0.1 s. Previous estimates have differed little from the present value.

P_b

The formal error on the orbital period is 60 μs, or nearly 2 parts in 10^9. The actual uncertainty is most likely a few times that. Because the orbital period is very poorly determined in one observing session, the actual value is dependent on the arbitrary offsets between the observing runs. A more accurate value will not be known until a relatively long interval of un-offset data is gathered. A more reasonable guess at the actual uncertainty would put it at ±100 μs, twice the formal error.

ω

The estimate of the longitude of periastron at time T_0 is also influenced by the fit to γ, though not as much as is $a_1 \sin i$. A discussion similar to the one concerning the interaction between γ and $a_1 \sin i$ is appropriate here. The actual value of ω may vary by several times the formal errors as different values of γ are assumed; however, the value associated with a specific value of γ is quite well determined.

$\dot{\omega}$

The final value of the advance of periastron is consistent with all previous determinations, and should be accurate to within the quoted error.

γ

One of the accomplishments of the current work is the preliminary determination of γ, from which the masses of the components can be calculated. γ is the fit parameter which measures the effects of gravitational redshift and transverse Doppler shifts. Though the ~5 ms magnitude of γ is large compared to uncertainties in arrival time measurements, the near degeneracy of this term with $a_1 \sin i$ has heretofore prevented any estimate of this parameter. The present formal error is about 50% of the estimated value, and this large fractional uncertainty is responsible for the increase of the formal error in the $a_1 \sin i$ term from previously published vales, when γ was not included in the fit as a free parameter.

sin i

The sine of the inclination angle between the orbital plane and the plane of the sky can be determined directly from the effects of gravitational propagation delay and non-ellipticities of the orbit. The amplitude of these effects is small, in the range of 20 to 100 μs, and the estimation of sin i determined in the fit is only marginally significant. An upper limit to sin i of about 0.8 is fairly well established. The linearization procedure in the least

squares fit routine apparently breaks down at the lower limit as sin i → 0.37, the smallest permitted value. Additional data from the 1978 October observing session should greatly decrease the fractional uncertainty in the sin i estimate.

$\dot{P}_b$

The estimate of the time derivative of the orbital period is consistent with the predictions of General Relativity. Our value has 50% formal errors. A long time baseline is of importance in the determination of $\dot{P}_b$, and it may be several years before a 10% measurement of the magnitude of this effect is possible.

$\dot{x}$ and $\dot{e}$

$\dot{x}$ ($\equiv$ d/dt $a_1 \sin i$) and $\dot{e}$ do not represent any known physical processes in the system and are included as checks on the model and quality of the data. They should both be consistent with zero, as is observed. The actual values of the derivatives do reflect effects of small systematic errors present in the early timing data.

C H A P T E R I I I

THE PULSAR

§1. Introduction

In this chapter we report on many diverse studies we have made of the pulsar. The major thrust of the data taking has always been acquisition of timing data; however, a significant effort has been expended in analyzing the data towards other ends. Some of these studies are of interest only in the understanding of PSR 1913+16 as a member of the class of pulsars (or the understanding of the class of pulsars itself). However, aspects of these studies do have bearing on the nature of the as yet undetected companion and other questions of concern about the binary system.

Section 2 present studies of the radio flux received from the pulsar, and discusses the possibilities and meanings of secular flux variations as well as dependencies of the flux with frequency and orbital phase. The third section is concerned with the dispersion measure and an investigation of its variation as a function of orbital phase. Section 4 is an investigation into the long term stability of the pulse shape, dependencies on observing frequency and orbital phase. Section 5 is a study of the polarization of the integrated pulse profile. And, finally, the sixth section reports the results of an unsuccessful search for a radio pulsar companion to the observed pulsar.

§2. Flux Density Studies

i) Determination of Flux Density.

The flux density from the pulsar is of little importance in the timing analysis of the system, and no absolute calibrations of the telescope system were made. However, it is possible to determine the flux density of the pulsar to fair relative accuracy from the known system temperature and system gain, and the measurable signal-to-noise ratio for each 5 minute average. Since the telescope pointing of the 430 MHz and 1420 MHz systems have remained virtually unchanged over the last 4 years, any large variations in flux can be interpreted as real variations of the pulsar flux.

The flux density was determined as follows. For total sky + system temperature T_{sys} in °K and system gain G_{sys} in °K/Jy, the flux density S_ν in mJy is

$$S_\nu = 1000. \frac{SN \cdot T_{sys}(\nu)}{G_{sys}(\nu)} N^{-1/2} \quad mJy \qquad \text{(III-1)}$$

where SN is the signal-to-noise ratio and N is the number of degrees of freedom. Both system temperature and system gain were corrected for telescope zenith angle dependencies where appropriate. Pointing errors at both frequencies constitute less than 10% errors. The number of degrees of freedom is established as follows:

$$N = n \tau \Delta\nu \, i \qquad \text{(III-2)}$$

where n is the number of polarizations (usually 1 at 430 MHz and 2 at 1420 MHz), τ is the RC smoothing time constant used, $\Delta\nu$ the detection bandwidth, and i the number of pulses in the average profile (about 5000 for a 5 minute integration). The signal-to-noise ratio was determined by dividing the on-pulse intensity by the off-pulse rms noise. The accuracy of this procedure was investigated by varying the off-pulse noise by smoothing the data at the analysis stage and recalculating the fluxes. The data point-to-point variations were about 10%, and the overall shift in flux levels around 20%. The errors have been taken to be 20%, though data smoothed with the same time constant may in fact have smaller relative errors.

ii) Pulsar Spectrum.

Two frequency observations were made in 1977 July - August, and from them a spectral index can be calculated. Assuming that a power law adequately describes the flux density over that frequency range, we have that the flux density at frequency ν S_ν is

$$S_\nu = S\nu^{-\alpha} \qquad \text{(III-3)}$$

where S is the flux density at a standard frequency and α the spectral index. For $S_{430} = 5.9\pm1.5$ mJy and $S_{1420} = .48\pm.13$ mJy (see Table III-1) we have $S_\nu = 1(\pm.25)\nu^{-2(\pm.5)}$ mJy for ν in gigahertz.

These values of S and α agree to within the errors with

Table III-1. Binary pulsar flux densities.

Observing frequency (MHz)	Observing run [1.] (Flux density in mJy)				
	Lyne & Ritchings [2.]	1976 Nov.-Dec.	1977 July-August	1977 December	1978 March-April
430	4.9 (1976 May)	5.4	7.7	---	---
1420	0.80 (1975 June)	0.63	0.55	0.98	1.08

Note 1. The standard errors for all the data are approximately 20%.

Note 2. (Lyne and Ritchings 1977)

the values determined by Lyne and Ritchings (1977). The observations of Lyne and Ritchings and those reported here both show signs of possible long term flux variations, which could explain the differences in S and α. The flux data reported here are very poorly calibrated, and are of more interest in studies concerned with variations rather than absolute calculations of flux and spectral index.

iii) Short Term Flux Variations.

The possibility exists that the flux from the pulsar might show periodic variations on the timescales of minutes to hours. Such a variation might be due to a classical neutron star precession (see Helfand et al. 1977 and references therein). The data were plotted on a point-by-point basis for each day, and on a day-by-day basis for each observing run, and searched by eye for periodicities. No significant flux variations were seen on timescales between 15 min and 15 days. Due to poor calibrations and inhomogeneous sampling rates, it is unlikely that a formal power spectrum analysis would reveal additional structure. A line plot of all the fluxes from 1978 March - April is reproduced in Figure III-1. The data of individual days are delineated and labelled.

iv) Orbital Variations of Pulsar Flux.

The flux from the pulsar has been searched for a dependency on orbital phase. Impetus for the analysis comes from the possibility of interactions of the emitted pulse

Figure III-1. Plot of all flux density measurements during the 1978 March - April observing run. Each point represents the flux of a 5 minute average. Days of the measurement are indicated, as well as time of transit of the pulsar for each day (designated "t"). Eclipse time by a hypothetical extended companion is marked "e". Point #1 bears representative error bars.

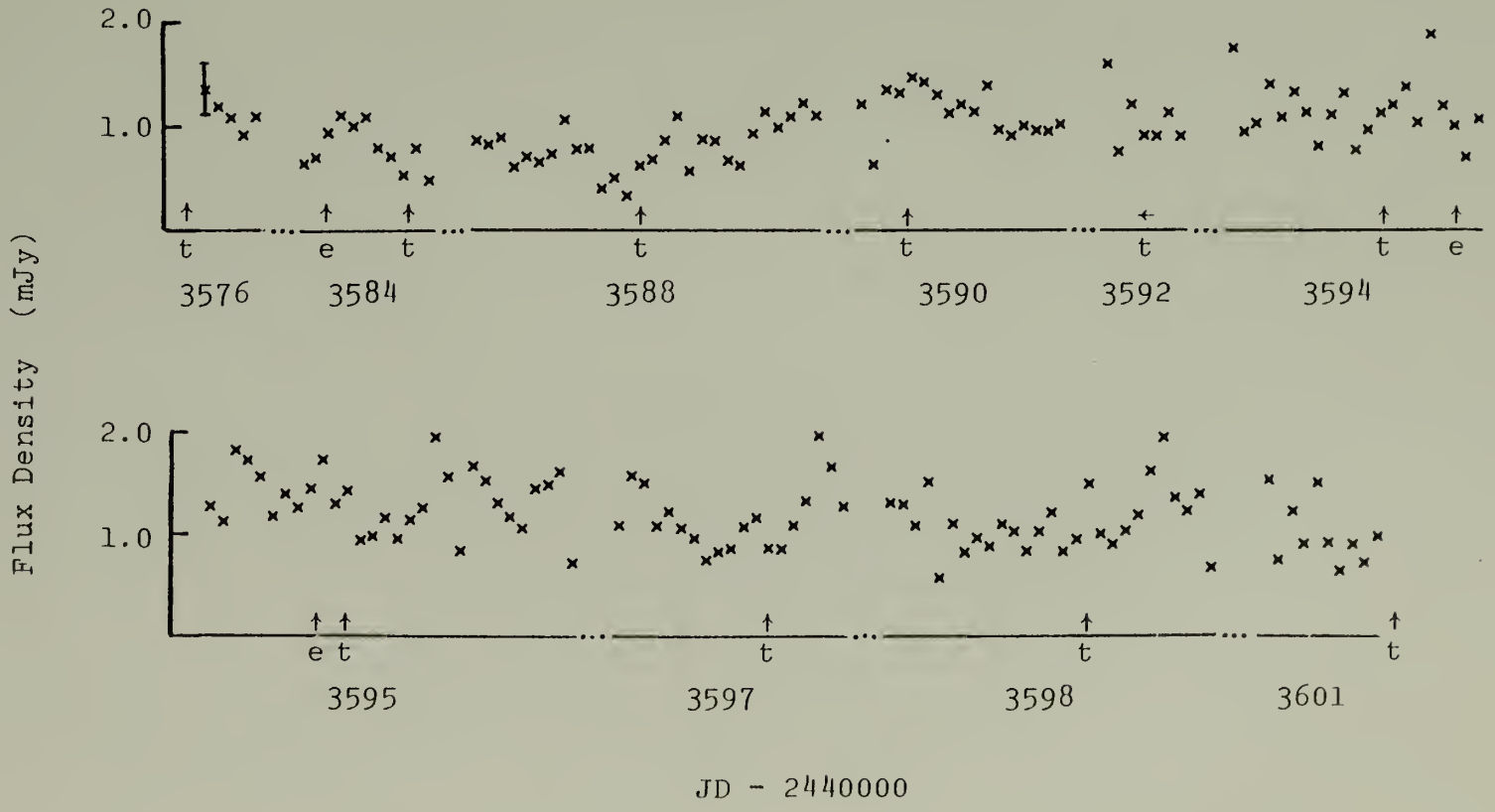
2.0
1.0
Flux Density (mJy)
t
e
t
t
t
t
t
e
3576
3584
3588
3590
3592
3594
2.0
1.0
e t
t
t
t
3595
3597
3598
3601
JD - 2440000

and companion object. One such interaction, the eclipse of the pulsar by the companion, is dealt with separately at the end of this subsection.

The average flux $\bar{S}_\nu$ and associated statistical deviation σ were computed for 8 orbital phase intervals. Each interval covered about 1 hour of the orbit, and interval #1 was centered on periastron. All the flux data for one observing run was used to determine a set of average fluxes for each phase interval. The different observing runs were then compared for correlations between maximum or minimum flux and particular phase intervals. The results of this comparison are to be found in Table III-2. None of the differences between maximum and minimum flux exceeded 1.6 times their combined statistical errors during and observing run, and there were no tendencies for these maxima and minima to associate with any orbital phase.

Eclipses

In the event that the inclination angle i between the orbital plane and the sky is greater than about 80°, and the companion star is a helium star ($R_{He} \sim .1 R_\odot$), we would expect about a 5 minute eclipse of the pulsar to occur at orbital phase .94. To look for eclipses, the exact phase of eclipse for each observation session was calculated, and the flux data searched by eye for signs of significantly smaller flux received at those phases. There were no such indications.

An eclipse by a white dwarf would last only about 1 minute and would probably not be detectable in a 5 min average.

Table III-2. Average flux density variations with orbit phase.

Observing run	freq. (MHz)	Maximum value (mJy)	Maximum bin #	Minimum value (mJy)	Minimum bin #	σ	Difference value (mJy)	Difference (in σ)
1976 Nov.-Dec.	430	7.10	1	6.13	6	~1.8	.97	.5
	1420	Insufficient orbital coverage						
1977 July-August	430	8.59	3	6.93	4	~2.0	1.66	.8
	1420	.63	5	.46	2	~.18	.27	1.5
1977 December [1.]	1420	1.14	8	.79	3	~.25	.35	1.4
1978 March	1420	1.19	1	.93	4	~.30	.26	.9

Note 1. Incomplete orbital coverage.
Phases .4 to .8 not sampled.

The inclination of the orbital plane to the sky would have to be greater than about 88.7° for a white dwarf companion to eclipse the pulsar.

v) Long Term Flux Variations.

As can be seen from Table III-1, the flux from a pulsar at the two frequencies shows signs of variability with time. These variations could be due to intrinsic changes in luminosity of the pulsar (see Helfand et al. 1977 for discussion and additional references) or they could be the result of pulsar precession. The precession is due to spin-orbit interactions and in General Relativity is predicted to be about $2^\circ\ yr^{-1}$. This precession is discussed further in chapter IV. In the absence of additional information, it is impossible to determine the source of the flux change. A correlation between flux variations and integrated pulse shape changes would greatly favor precession as the explanation.

§3. Dispersion Measure

The dispersion measure quoted in the discovery paper was 167±5 pc cm^{-3}. Two frequency timing measurements have improved the value to the current estimate of 171.64±.01 pc cm^{-3}. Between 1420 MHz and 430 MHz, the dispersive time lag is about 3.5 seconds. The two frequency rms residuals of the 1977 July - August data are about 200 μs. If the error in DM accounted for all of this residual, the quoted value would be in error by almost ±.01 pc cm^{-3}. It should be

noted that the dissimilarity of the mean pulse profile at the two frequencies introduces an arbitrariness of several hundred μs in arrival time of the same pulse at the two frequencies. This arbitrariness can introduce an error of roughly 0.01 cm^{-3} pc in the DM. For further discussion of interstellar dispersion and dispersion measures, please refer to Manchester and Taylor (1977).

Dispersion at the Pulsar

If there is a high electron density around the companion (caused by mass loss or an extended atmosphere), pulses emitted by the pulsar on the far side of the orbit will undergo more dispersive delay than those emitted on the near side. The exact variation of the dispersion measure is strongly model dependent. Also, the timing data fit to the orbital parameters will remove much of the variation if only single frequency data is used, because the added delay will be interpreted as new values of the semimajor axis, eccentricity, time of periastron passage, or longitude of periastron. Two frequency observations prevent the fit from removing the dispersive delay, because of the strong frequency dependence of the dispersive delay. The effect of the variable dispersion would show as either increased residual noise at specific orbital phases, or significant disagreement between final values of the orbital elements for least squares fits to data of each frequency separately.

Tests with generated data were performed to determine the sensitivity of the data to electrons inside the orbit.

A set of arrival times for an entire orbit were generated at 430 and 1420 MHz. To these arrival times was added zero mean gaussian noise with an rms residual of ~120 μs, comparable to the rms residual of the 1977 July - August data. The arrival times were then delayed by the amount appropriate for the observing frequency and the average line of sight electron density from the pulsar position at each arrival time. The electron density was modeled in 2 ways. Model 1 had a uniform electron density of 10^6 electrons cm^{-3}. Model 2 had an electron density that varied as the inverse square of the distance from the companion, as is found in the case of the sun. The average electron density inside 1 light second (approximately the closest approach) was once again 10^6 electrons cm^{-3}, and the density rose to a maximum of $\sim 3 \times 10^7$ electrons cm^{-3} at the surface of a hypothetical .1 $R_\odot$ helium star.

Figure III-2 shows residuals before and after the fit for a uniform density background of electrons. The ability of the fit parameters to absorb the added delay is frightening. The 1.8 ms maximum delay was reduced to an excursion not visible above the noise. The semimajor axis and eccentricity were changed by less than 1 part in 10^3 to accommodate the added delay. Figure III-3 also shows residuals from the same fit using two frequency data. The effects of the 10^6 electrons cm^{-3} are obvious, and as little as 10^5 electrons would be easily detected, at any inclination angle permissible for a helium star companion ($i \geq 50°$).

Figure III-4 shows residuals of 430 MHz data with 120

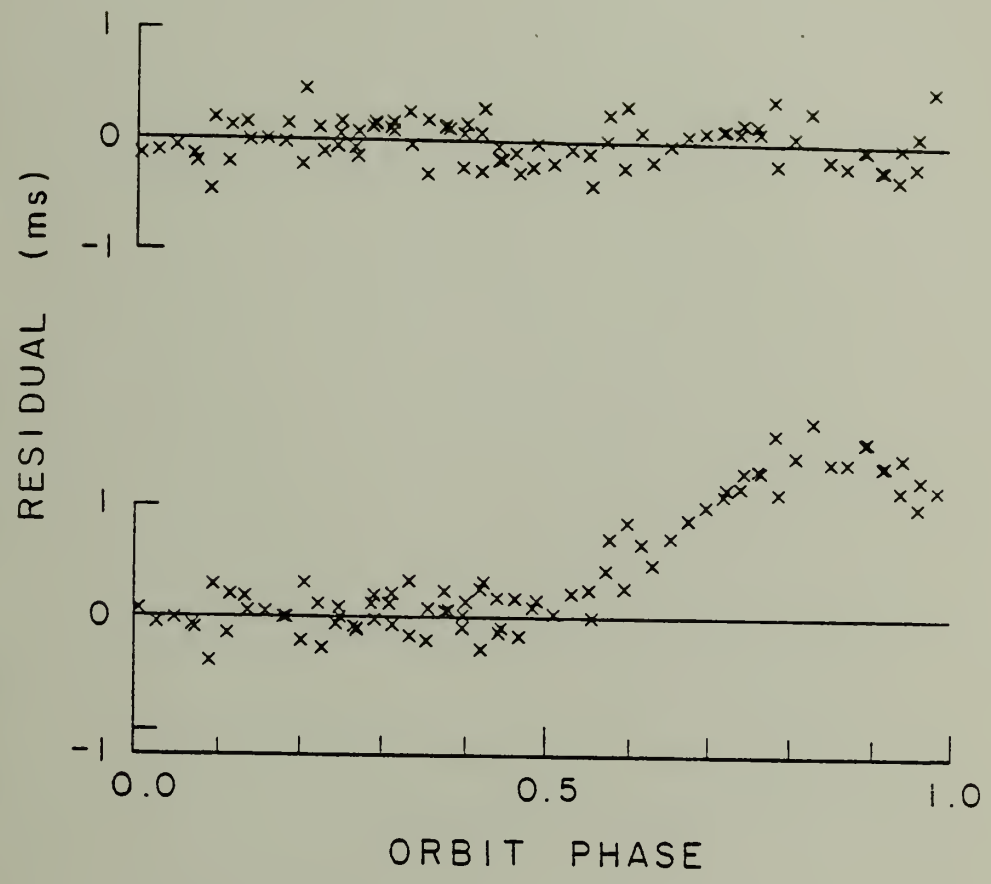

Figure III-2. Plot of 430 MHz residuals from generated arrival time data for uniform density electrons inside the orbit of the pulsar. The upper plot shows after the fit residuals. The lower plot shows the actual size of the added delay before the fit.

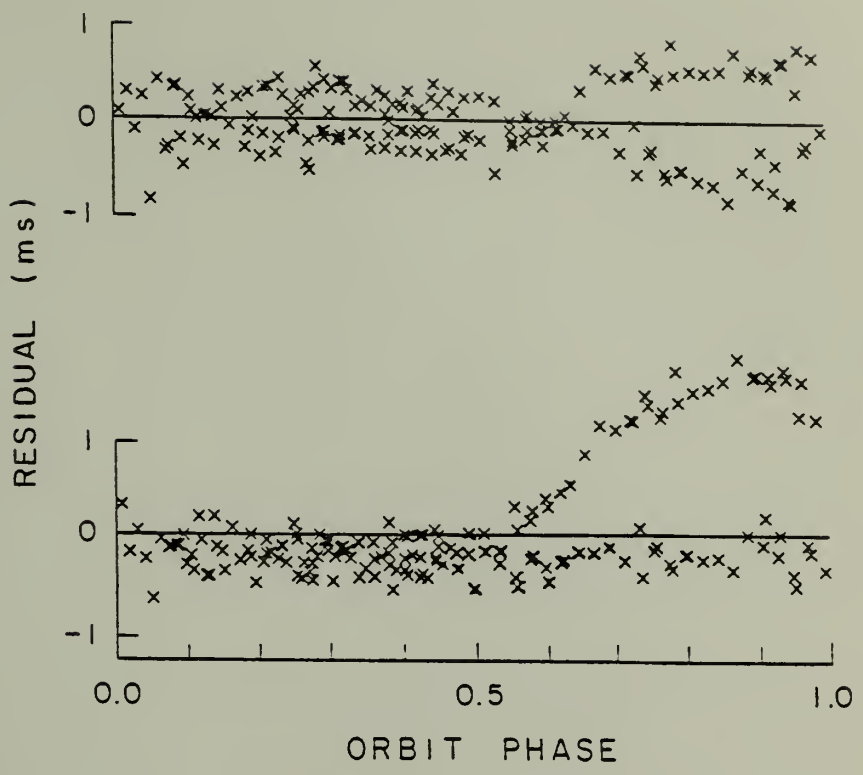

Figure III-3. As in Figure III-2, except that data at 1420 MHz was included.

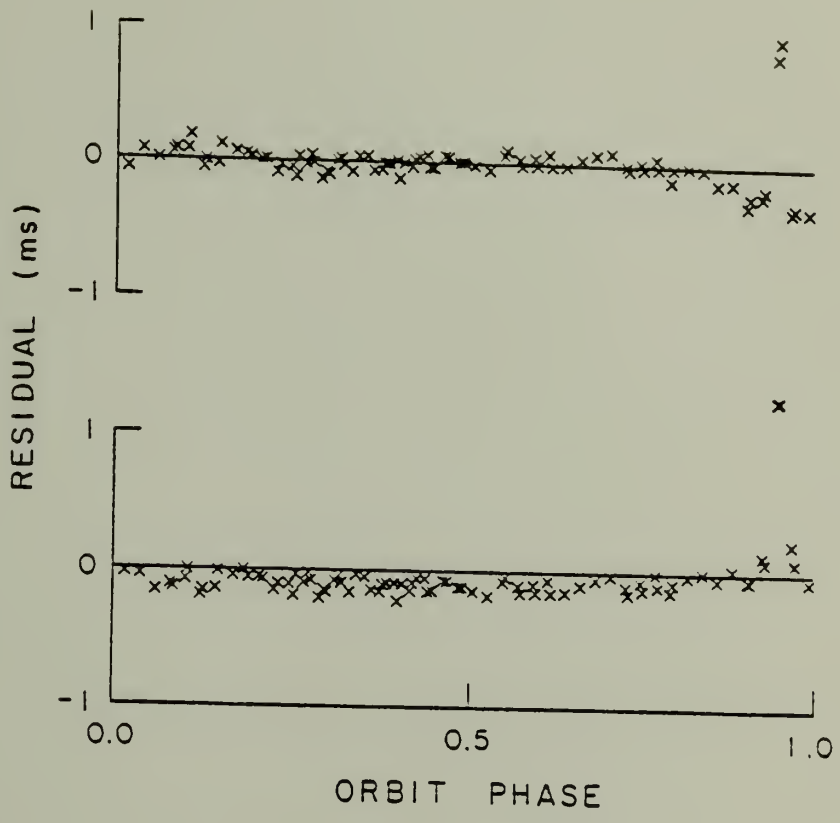

Figure III-4. Plot of 1420 MHz residuals for an inverse square dependence of electron density. Upper and lower plots the same as Figure III-2.

μs rms gaussian noise and an added dispersive delay appropriate for electrons whose density varies as the inverse square of the distance from the companion. Because the very sharp increase occurring near eclipse is so unlike the dependencies of the orbital parameters, the effect is not removed by the least squares fit. Consequently, an average electron density of as small as 10^4 electrons cm^{-3} would be detectable if the inclination of the orbit was about 90°. This upper limit increases to about 3×10^5 electrons cm^{-3} when the orbit is tilted at 60° inclination angle.

From the results of these two limiting cases, we conclude that we should be able to detect an average electron density of about 10^5 electrons cm^{-3}. This upper limit can be used to set restrictions on mass loss from a hypothetical helium star companion. Using the equation in section IV of Smarr and Blandford (1976), hereafter referred to as S & B, we have that the electron density n_e is

$$n_e \sim 3 \times 10^8 \dot{M}_{10} V_8^{-1} \text{ cm}^{-3} \qquad \text{(III-4)}$$

where $\dot{M}_{-10}$ is the mass loss from the helium star in 10^{-10} $M_\odot$ s^{-1} and V_8 is the stellar wind velocity in 10^8 cm s^{-1}. The established electron density limit forces

$$\dot{M}_{10} V_8^{-1} \lesssim 3 \times 10^{-4} M_\odot \text{ cm}^{-1} \qquad \text{(III-5)}$$

The values for $\dot{M}_{-10}$ and V_8 are greatly restricted, but a mass loss rate of $\dot{M}_{-10} = 10^{-3}$ $M_\odot$ s^{-1} and wind velocity $V_8 =$ 3 cm s^{-1} would be within the limits described by S & B. It

is also possible for mass loss and wind velocity to be substantially larger than the limits determined above. If the luminosity of the pulsar is sufficiently high, the electrons may be swept clear of the system.

§4. The Mean Pulse Profile

A natural consequence of the arrival time calculation described in chapter II was the creation of standard profiles for each observing run. The standard profiles were an aligned sum of all the good data obtained during an observing run, and give an accurate picture of the mean pulse profile at each frequency. Figure III-5 shows the 1977 July - August 430 MHz profile and Figure III-6 shows the 1978 March 1420 MHz profile.

The variation of pulse shape with frequency appears to be quite normal. At 430 MHz, measuring from the center of the first peak, the middle peak is 4.67 ms later and the final peak is 6.8 ms later. The overall pulse width (at the 10% intensity level) is 9.9 ms, giving a rather large duty cycle of 17%. At 1420 MHz, the pulse profile is both narrower and more symmetric. Only the two outer peaks are present, now at almost equal intensity. The trailing peak is 6.4 ms behind the leading. To the 10% level, the 1420 MHz pulse width is 8.3 ms.

Pulse components in general follow a rough rule that the pulse width W varies as a weak power of the frequency ν (Manchester and Taylor (1977), hereafter referred to as

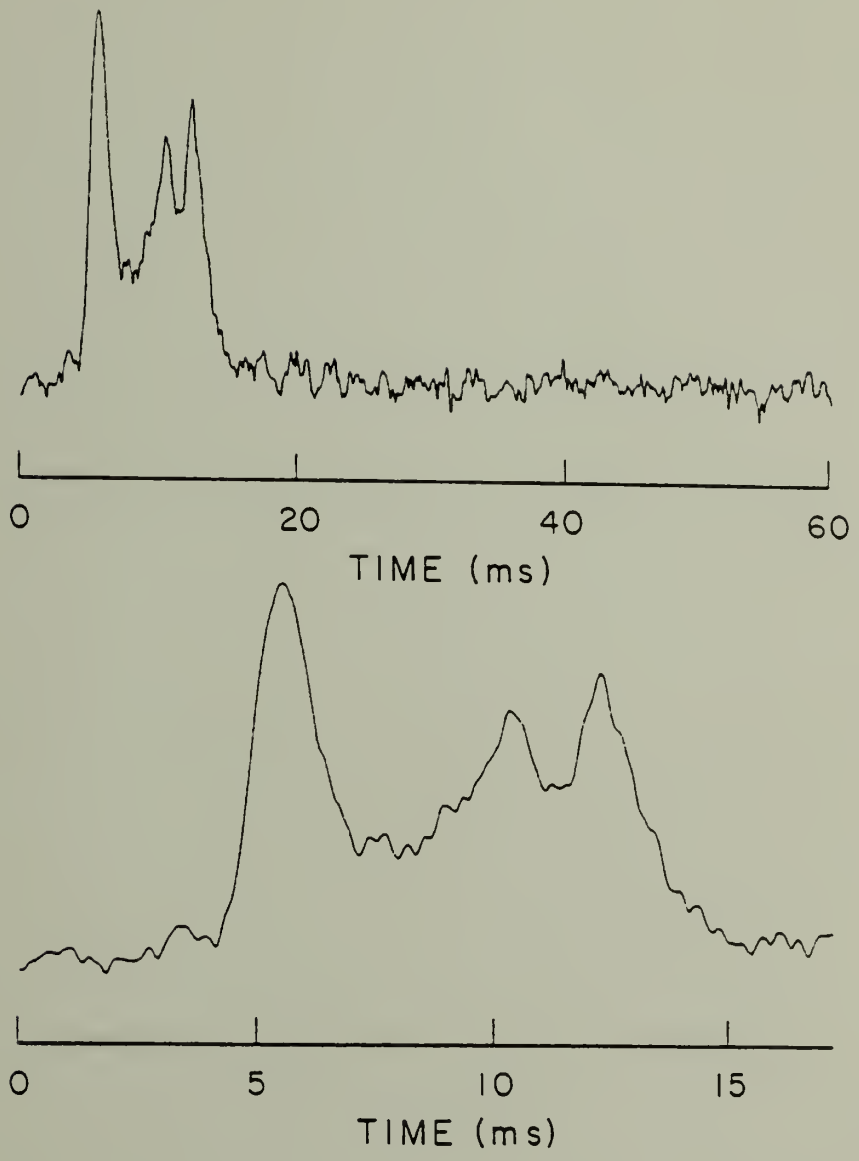

Figure III-5. The 430 MHz profile of 1977 July - August. The upper plot shows the entire period. The lower plot shows an expanded plot of the pulse. 60 5 minute averages were summed to produce the plot.

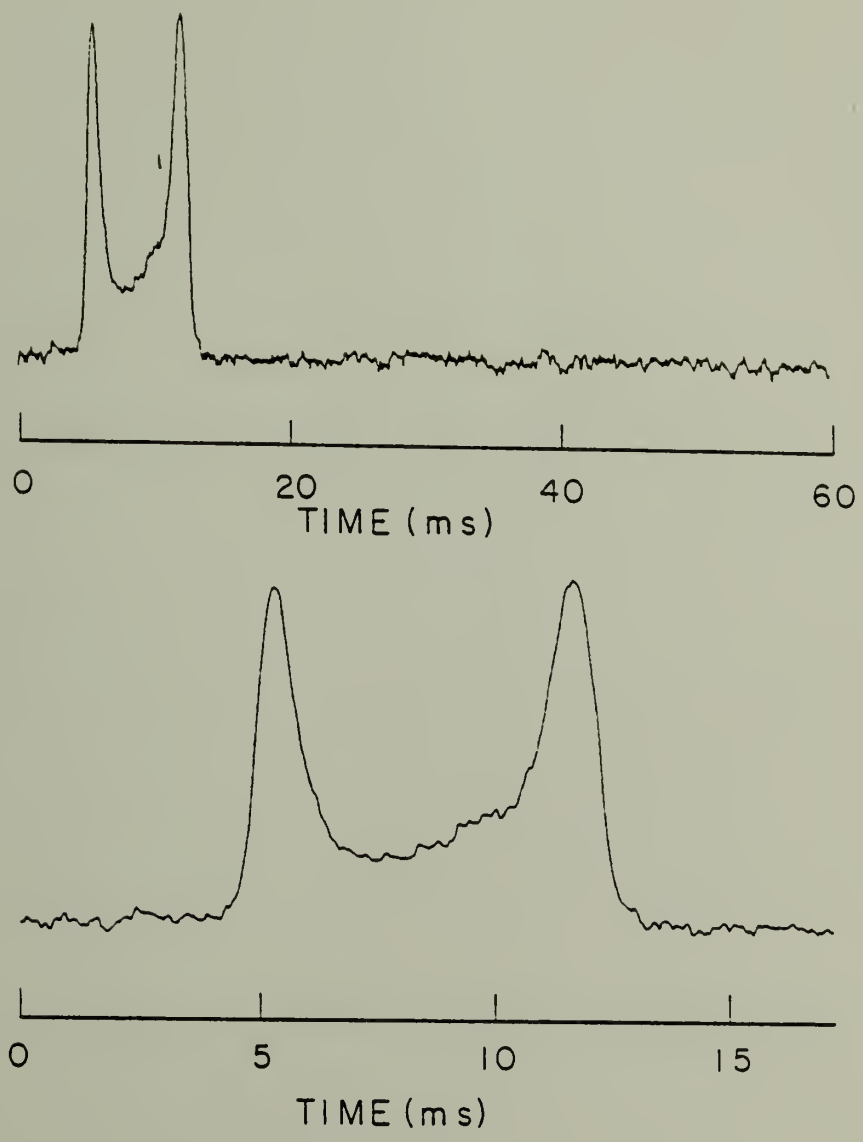

Figure III-6. As in Figure III-5 for 1978 March - April 1420 MHz data. There are 75 5 minute averages in the plot.

M & T)

$$W \sim \nu^{-p} \qquad \text{(III-6)}$$

where the separation index p has a value of -.25±.11 over the sample of pulsars in chapter 2 of M & T. For PSR 1913+16 the peak-to-peak separation at the two frequencies yields a separation index of -.50, somewhat steeper than other pulsars.

There is possibly an indication of a scattering tail to the two outside peaks of the 430 MHz profile. For the first peak, the rise time is about 0.58 ms from the 30% to the 90% level. The corresponding fall time on the trailing edge of the same peak is closer to 0.92 ms. Assuming a symmetrical unscattered peak suggests that the scattering tail has a 1/e width of about 0.6 ms.

The profile can be treated as an unscattered profile convolved with a truncated exponential.

$$g(t) = \begin{cases} \exp -(2\pi \Delta\nu)t & t \geqslant 0 \\ 0 & t < 0 \end{cases} \qquad \text{(III-7)}$$

where $\Delta\nu$ is the scintillation decorrelation bandwidth. The scintillation bandwidth is best determined empirically from Figure 7.9 of M & T:

$$\Delta\nu \sim \nu^{4}\ DM^{-2.5} \qquad \text{(III-8)}$$

where the errors on the exponent of the dispersion measure are ±.5. From these considerations we expect the dispersion

tail to have a width of somewhere around 0.5 ms, in rough agreement with the observations. There is no scattering at the higher frequency.

Phase Variations of Pulse Shape

An attempt was made to detect variations in the mean profile shape as a function of orbital phase. Variations have previously been investigated by Gullahorn (1978); however, his results were inconclusive due to the much poorer quality of his data. We have obtained 8 average profiles around the orbit for each observing session. Each phase profile was then differenced against the grand average for the observing run, and the phase average, grand average, and difference profile plotted out for inspection.

There are several ways in which the pulse shape could have an orbital phase dependency. The simplest is smearing. The inaccuracy of the pulsar periods used to fold the data will have a strong phase dependence, being 10 to 100 times worse around periastron. The contamination of the grand average profile by the smeared profiles will cause the difference profiles to be non-random throughout the orbit. There is evidence of smeared pulse shapes in the 1977 July - August and 1977 December data.

There are two shape varying processes which are intrinsic to the data. The first is Galilean aberration (S & B). A distant observer will receive a pulse from the pulsar only if the pulse is emitted slightly backward from the line of

sight to compensate for the motion of the pulsar. The major effect is a slight timing error of order 10 μs. As the angle is a function of the orbital velocity, the observer will also see slightly different cuts through the emitted beam, which could result in small shape changes. The effect should not be detectable. Likewise of negligible importance is a phase dependent mean pulse shape arising from the variation of the emitted frequency for a fized observing frequency. Because the pulsar is moving with respect to the interstellar medium, a fixed observing frequency is the Doppler shifted result of a range of frequencies emitted by the pulsar. Any strong dependency of mean pulse shape on frequency will be translated into a dependency upon Doppler shift, and hence orbital phase. The frequency excursion is about 0.5 MHz at 430 MHz.

Additionally, a variable amount of scattering around the orbit due to the presence of free electrons would modify the pulse shape. However, the limit to electrons established in the last section obviates this effect. There is also the possibility that the pulsar interacts with the companion star.

Plotted in Figure III-7 is the grand mean pulse shape and 8 difference profiles. These are 1415 MHz profiles from the 1978 March - April session. The only difference profiles with noticeable trends are phase bins 3 and 4, orbit phase .19 to .44. The features beneath the first peak have two- and three-σ heights against the noise, respectively. A

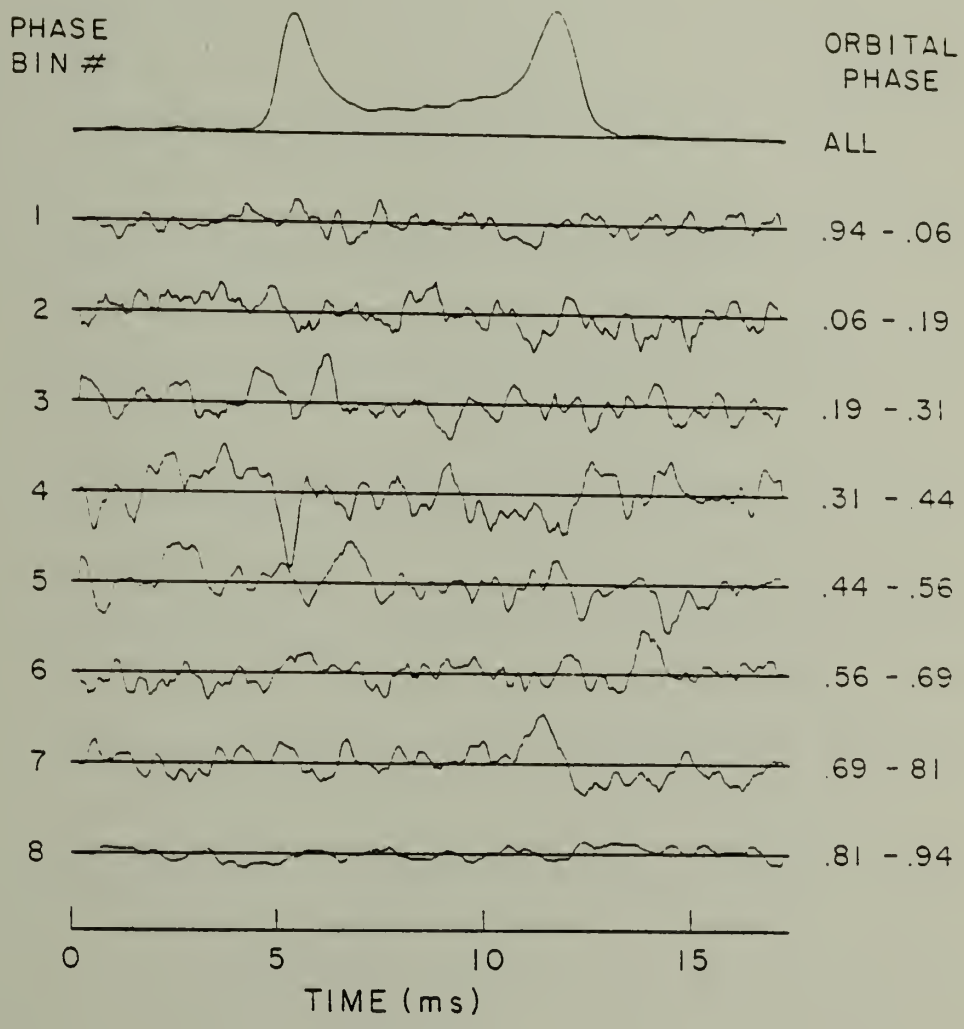

Figure III-7. The 1978 March - April standard profile and 8 orbital phase difference plots. Phase bin numbers 1 and 8 had significantly more 5 minute averages. Consequently the noise in these difference profiles is smaller than in phase bins 2 - 7.

shift of about 50 μs would be required to explain a spike the size of the down-pointing feature of phase bin #4, and such a shift is probably accounted for by random errors of the alignment of the pulses introduced by noise. The orbital phases covered by those two phase bins should not be particularly sensitive to either intrinsic or introduced variations. The good behavior of the difference profiles around periastron (1, 2, and 8) is additional confirmation that smearing in the 1977 March - April data is small.

§5. Polarimetry

There are several reasons for studying the polarization of the pulsar. The signal is too weak for single pulse analysis, but the percentage of linear and circular polarization and linear position angle can be determined for the integrated pulse profile. These quantities are of interest in any pulsar, but can take on even more significance for the binary pulsar. In the event that the pulsar precesses, the observer's line of sight will describe a series of different cuts through the emission beam of the pulsar. Any changes in percent polarization or sweep of position angle in the integrated pulse profile then supply us with the first two dimensional map of these characteristics.

The polarimetry observations were made 1977 August. Data was taken at 1415 MHz and 430 MHz. The 1415 MHz data was summed on-line and recorded in a fashion similar to the timing data. It was not possible to sum the 430 MHz data

on-line. As will be described below, the 430 MHz signal was fast-sampled and the final folding completed in Amherst.

In order to determine the polarization of the integrated profile, it is sufficient to determine the Stokes parameters I, Q, U, and V across the profile. (The definitions of the Stokes parameters and an explanation of their use can be found in Appendix II.) The observatory maintains a 30 MHz IF adding polarimeter. The input to the polarimeter consists of the LHCP and RHCP signals from the sky, and the output are 2 circular polarizations LHCP and RHCP again and 2 linears, LHCP + RHCP and RHCP - (LHCP delayed by $\pi/2$). From these four quantities, the four Stokes parameters can be constructed. The determination of the Stokes parameters from the polarimeter output and the calibrations are also described in Appendix II.

i) The 1415 Observations.

The LHCP and RHCP signals at 1415 MHz were down-converted to 260 MHz, passed through a 5 MHz filter, and finally down-converted to 30 MHz IF and sent to the polarimeter. The four outputs were separately detected by square law detectors, digitized, and folded on-line, as described in the last chapter. The dispersive smoothing across 5 MHz at 1415 MHz is about 2.5 ms. The signal was smoothed by a .5 ms RC time constant.

ii) 430 MHz Observations.

Due to the ν^{-3} frequency dependency of dispersive

smearing across any given filter it was not possible to simultaneously acquire sufficient bandpass and limit the dispersive smearing to less than the pulse width with available single filters. So on-line summing was abandoned, and the data was fast sampled in the following fashion. The LHCP and RHCP signals from the sky were mixed down to 30 MHz IF and fed to the polarimeter. The 4 outputs were sent to the 64 channel 250 kHz filterbank in the 4 × 16 mode. From each polarization set of 16 channels, the middle 4 were tapped off, smoothed by a .5 ms time constant and sampled at a 1 ms sampling rate, and written out on magnetic tape. The observatory fast sampling program can accept only as many as 16 simultaneous inputs, so only four channels for each polarization could be used.

In Amherst, the fast-sampled data were folded and then the Stokes parameters calculated as described in Appendix II. At 430 MHz, the smearing across one 250 kHz filter is 4.25 ms, so the final profile has only 3 or 4 independent points across it.

Results

The pulsar signal is about 25% linearly polarized at 430 MHz (as an average polarization for the pulsed emission). There is no circular polarization to the 10% (3σ) level. See Figure III-8 for plots of I, $(Q^2 + U^2)^{1/2}$, V, and position angle across the pulse. The presence of the linear polarization and absence of circular polarization is typical of most pulsars. The position angle is not referenced to

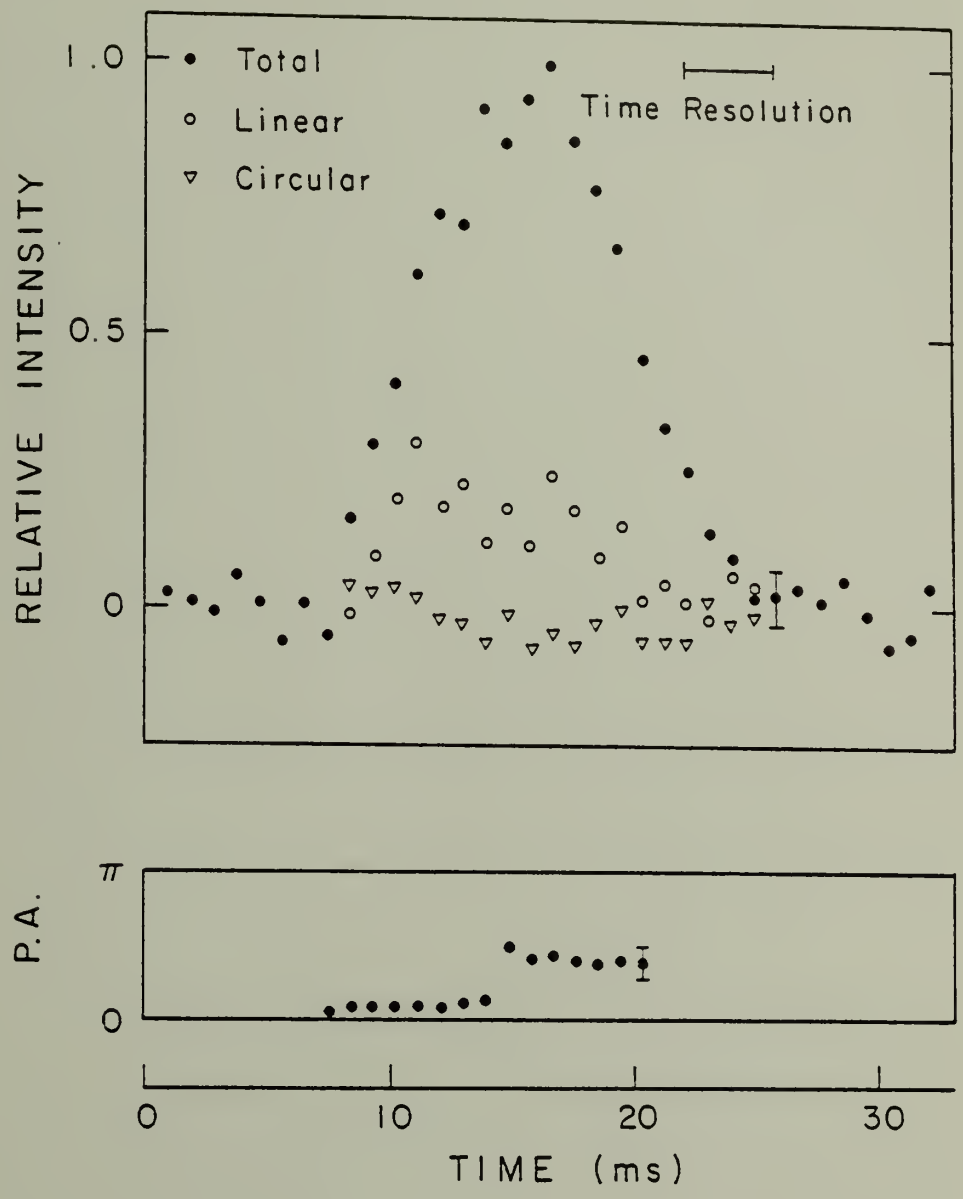

Figure III-8. The 1977 August polarimetry observations. The average profile is shown in total intensity, linear, and circular polarizations at 430 MHz. The lower plot shows position angle across the pulse. Approximate 3σ error bars are indicated.

the sky and the scale has an arbitrary zero point.

The absence of detectable polarization at 1415 MHz is also typical of pulsars. Depolarization usually occurs at higher frequencies. However, the source is weaker at the higher frequencies and the 80 min of data permit only a 3σ upper limit of 30%. The same percentage polarization seen at 430 MHz would have only been marginally detected at 1415 MHz, so the non-detection is not surprising.

§6. Search for the Companion

The nature of the companion object to PSR 1913+16 is of great interest. If the companion can be treated as a point mass, there are several interesting General Relativity tests and observations that can be made. In addition, if the companion were another pulsar, the ratio of the masses in the system could be determined directly from the amplitudes of the velocity curves.

It is entirely possible that a companion pulsar would not have been detected. The search program that discovered the binary system only reported the detection of the highest signal-to-noise periodic signal. A weaker pulsar at the same position would not have been found. All data taken subsequently were folded at the period of PSR 1913+16, and would not have been sensitive to any other periodicities. However, the fast-sampled data taken by Hulse in 1974 has been re-examined for other periodic signals.

The fast fourier transform algorithm was used to

CHAPTER IV

TIMING RESULTS AND GRAVITATIONAL THEORY

§1. Introduction

This chapter is a discussion of the results of the previous two chapters. The emphasis is on the pulsar timing results in particular. The values obtained from the timing data for the pulsar, orbital, and relativistic effects are discussed within the context of General Relativity and, where appropriate, other currently viable gravitational theories.

In the next section, the method by which the pulsar and companion mass can be determined is presented. The information content of the first three orders in (v/c) is also discussed and physical interpretations are given. In section 3, the possible causes of the observed advance of periastron are discussed, and the fourth section discusses the possibility of detecting the effects of gravitational quadrupole radiation. The precession of the pulsar beam is discussed in section 5, and the final section examines the utility of the binary system as a laboratory for testing currently viable metric theories of gravitation.

§2. Determination of the Masses

This section describes in detail the method by which the individual masses of the components of the system may be calculated, and the inclination angle and orbital elements of the binary system completely determined. The calculations

compute the power spectrum of about 20 hours of data. The original sampling was 2 ms per sampling interval. The apparent sampling was increased to 4 ms/interval and 16 ms/interval by summing the appropriate number of consecutive data points so that the transformed power spectra would adequately cover the range of pulsar periods. The power spectrum was computed for sets of 16,384 points. Because the companion's instantaneous velocity depends on the unknown mass ratio of the two stars, the power spectra were summed into one of ten different arrays according to the pulsar velocity. These sums were later combined into different grand sums with the spectra compensated for different assumptions of the mass ratio. Ratios were chosen such that $0 < M_p/M_c < 10$. There was no evidence in the final grand sums of any periodic signal except that of PSR 1913+16 and the 60 Hz power line and their harmonics. Between the two sampling rates, possible pulsar periods between 8 ms and 10 s were covered. We estimate that our minimum detection level was 60 μJy at 3σ of the noise. We conclude that the companion either is not a pulsar or its emission is not beamed at the earth.

to be discussed make use of information about the orbital elements and relativistic effects present in $O(v/c)$, $O(v/c)^2$, and $O(v/c)^3$ terms that describe the delays in the pulse arrival times. As the orbital velocity of the companion is approximately .001 c and the orbital diameter a few light-seconds, these effects are present in the data on the second, millisecond and microsecond timescales, respectively.

i) The $O(v/c)$ term.

The $O(v/c)$ term is the well-known Doppler shift. The observed pulsar period P_{obs} is related to the rotational period of the pulsar P_{em} by

$$P_{obs} = P_{em}\left(1 + \frac{V_{rad}}{c} + C\right) \qquad \text{(IV-1)}$$

where v_{rad} is the instantaneous radial velocity of the pulsar with respect to the observer at the emission of the pulse and C is an unmeasurable constant (absorbing relative motion between the two barycenters and redshift from the pulsar surface to infinity). Negative velocity indicates motion towards the observer. The delay in the arrival time is then the integral of the Doppler-shifted pulsar frequency and can be as much as ±2 seconds. The $O(v/c)$ term allows determination of the 5 orbital parameters of Table III-3, $a_1 \sin i$, e, T_0, P_b, and ω. Only the projection of the semi-major axis along the line of sight is determinable, because the radial velocity contains no information of transverse motions within the system.

ii) The $O(v/c)^2$ term.

The $O(v/c)^2$ term in the fit does contain information about transverse motions in the system. The term consists of a component due to the transverse Doppler shift (the apparent time dilation in an object moving with respect to the observer) and another due to gravitational redshift. The variable gravitational redshift is caused by the pulsar moving in and out of the gravitational well of the companion in eccentric orbit. Both of these effects depend on absolute motions within the system. With additional information, the $O(v/c)^2$ term can be used to determine a_1 directly.

However, in the absence of advance of periastron, the $O(v/c)^2$ term is exactly degenerate with the $O(v/c)$ term. This can best be seen by once again considering the effect of the two terms on the pulsar period. This development is adapted from Will (1979).

For an elliptical orbit, P_{obs} is related to P_{em} in the following fashion

$$P_{obs} = P_{em}\left\{1 + K_1(\cos(\omega+\phi) + e\cos\omega) + B\cos\phi + C + O\left(\frac{v}{c}\right)^3\right\} \quad \text{(IV-2)}$$

where ϕ is the true anomaly of the pulsar and K_1 and B are the first and second order coefficients.

$$K_1 = \frac{2\pi a_1 \sin i}{P_b c (1-e^2)^{1/2}} \qquad B = \frac{G M_c^2 (M_p + 2M_c) e}{c^2 M_T^2 a_1 (1-e^2)} \quad \text{(IV-3)}$$

As can be seen, K_1 depends on the observer's line of sight, whereas B is determined solely by the internal dynamics of

the system with $B/K_1 \sim v/c$. However, in the absence of periastron advance ($\omega = \omega_0$), the K_1 and B coefficients have exactly the same ϕ dependency, and cannot be separated in the fit. It is only in the presence of periastron motion over an appreciable section of the orbit that the two coefficients can be separated. In the fit routine, $a_1 \sin i$ is solved for rather than K_1. The second order effect is γ:

$$\gamma = \frac{2\pi a_1^2 e}{c^2 P_b}\left(2 + \frac{M_p}{M_c}\right) \qquad \text{(IV-4)}$$

which can be simply related to the coefficient B above.

iii) Determination of the System.

The following discussion is adapted from Taylor et al. (1976). In order to gain a complete dynamical understanding of the binary system, we need to determine independently the masses M_p and M_c, the semimajor axis a_1, and the orbit inclination i. Two relations between these four quantities are immediately available, as the projected semimajor axis,

$$a_1 \sin i = 2.345 \text{ s} \qquad \text{(IV-5)}$$

and the mass function,

$$f_m = \frac{(M_c \sin i)^3}{M_T^2} = \frac{4\pi^2}{G}\frac{(a_1 \sin i)^3}{P_b^2} \simeq .1312\, M_\odot \qquad \text{(IV-6)}$$

are determined by the $O(v/c)$ terms. A third relation is supplied by γ, the $O(v/c)^2$ term. The fourth relationship is provided by the periastron advance. If $\dot{\omega} = \dot{\omega}_{GR}$, then we have from the observed periastron advance:

$$M_T = M_p + M_c = 2.840\ M_\odot \qquad \text{(IV-7)}$$

The preceding discussion can be summarized by casting the equations into a form depending explicitly on γ. As γ is the least certain of the orbital and relativistic effects, the uncertainty in γ will dominate the other uncertainties, so that writing the equations in this form will facilitate error analysis. For convenience we define

$$Z = \left(2.016 + \frac{\gamma}{7.299\times10^{-4}\,s}\right)^{1/2} \qquad \text{(IV-8)}$$

Then the desired equations are:

$$\begin{aligned} M_p &= (4.261 - Z)\,M_\odot \\ M_c &= (Z - 1.420)M_\odot \\ a_1 &= 2.292\,(Z - 1.420)\,s \\ \sin i &= \frac{2.345}{2.292\,(Z - 1.420)} \end{aligned} \qquad \text{(IV-9)}$$

It is important to bear in mind that equations IV-8 and IV-9 are based on the assumption that the companion behaves dynamically as a point mass. The validity of this assumption is discussed extensively in the next section. In the near future, additional observations should be available. The anticipated increase in timing resolution may make it possible to solve directly for the inclination angle from the $O(v/c)^3$ terms. If this is the case, then the system is over-determined and we have an important check on the validity of the

assumption.

The present best fit value for γ is (from Table III-3)

$$\gamma = .0069 \pm .0030$$

which gives

$$\begin{aligned} M_p &= (.87 \pm .6)\, M_\odot \\ M_c &= (1.97 \pm .6)\, M_\odot \\ a_1 &= (4.51\ ^{+1.2}_{-1.6})\ s \\ \sin i &= (.52\ ^{+.27}_{-.12}) \end{aligned} \qquad \text{(IV-10)}$$

The current values are consistent with a system having two neutron stars of approximately the same mass. Such a system is the most likely on evolutionary grounds as well (but see chapter V section 2). Figure IV-1 displays the current estimates of the masses on a plot of mass vs. inclination angle.

iv) <u>The $O(v/c)^3$ Term.</u>

If the measurement error in a 5 min average profile can be made as small as 30 μs or so, as seems to be the case for the Swept L.O. data, then it should be possible to obtain information on the inclination angle from the $O(v/c)^3$ terms present in the data. The two most important effects at this level are the gravitational propagation delay and the post-Newtonian deviations from an elliptical orbit (Epstein 1977).

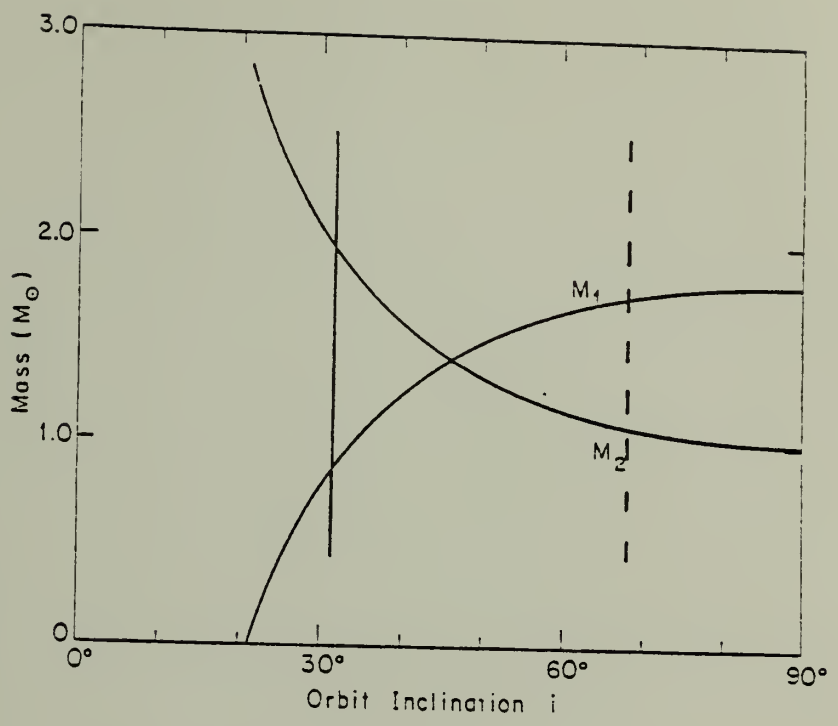

Figure IV-1. The mass of the pulsar, M_1, and companion, M_2, plotted as a function of the orbital inclination angle i, for the case when $\omega = \omega_{GR}$. The region to the left of the dashed line indicates the mass range allowed by the formal errors associated with the relativistic parameter γ. Best current values of M_1 and M_2 are found at the intersection of the solid line and the two mass curves.

The ability to obtain an independent measurement of sin i is critically important. The determination of the masses presented in the previous paragraphs was based on the assumption that $\dot{\omega} = \dot{\omega}_{GR}$. The redundancy provided by the $O(v/c)^3$ term allows a check to be made of this assumption. Such a consistency check has been obtained to some degree. Small values of γ certainly seem to be inconsistent with the derived value of sin i. The measurement error is still somewhat too large with the present data. A firm lower limit on sin i (i.e. large γ) has not been obtained, apparently because the linearization procedure breaks down in the fit. Additional timing data should remedy the situation.

§3. Advance of Periastron

The first relativistic effect to be detected in the binary system was the advance of periastron (Taylor 1975). The magnitude of the effect had been anticipated in the discovery paper, and in several early theoretical papers published shortly thereafter (Esposito and Harrison 1975, Brecher 1975, Hari Dass and Radhakrishnan 1975). The predictions were made on the assumption that the components behave dynamically like point masses, and that General Relativity is a valid description of gravitation. The agreement between prediction and observation is a strong indication that the companion does behave like a point mass (i.e. is a neutron star, black hole, or slowly rotating white dwarf). However, subsequent theoretical investigations have shown

that tidal or rotational distortions of an extended companion could give rise to a classical periastron advance of approximately the same magnitude. The following is a short discussion of these three possible causes of the observed 4.22°/yr advance of periastron.

i) General Relativity.

In General Relativity, the predicted periastron shift is

$$\dot{\omega}_{GR} = 2.104 \left(\frac{M_T}{M_\odot}\right)^{2/3} \text{ yr}^{-1} \qquad \text{(I-1)}$$

If $\dot{\omega} = \dot{\omega}_{GR}$, we have determined the total mass of the system:

$$M_T = (2.840 \pm .003)\, M_\odot \qquad \text{(I-2)}$$

This is the first instance where General Relativity has been used to make a precise astronomical measurement (Will 1979).

ii) Tidal Interactions.

If the companion is a helium star, there will be a classical advance in the longitude of periastron caused by tidal distortions induced in the companion by the pulsar's gravitation field (Masters and Roberts 1975). The tidal advance $\dot{\omega}_t$ is (Kopal 1959)

$$\dot{\omega}_t = (3.44 \times 10^6)\, k_2 \left(\frac{R_c}{R_\odot}\right)^5 \left(\frac{M_P}{M_c}\right) \left(\frac{M_T}{M_\odot}\right)^{-5/3} \text{deg yr}^{-1} \qquad \text{(IV-11)}$$

where k_2, the apsidial motion constant, is a measure of the distortion of the companion and R_c is the radius of the companion. Roberts et al. (1975) have made model calculations of helium stars of mass .5, .75, and $1M_\odot$ and determined that

the combined classical and relativistic advance of those systems would be similar to the observed values. There are several important observational tests for a helium star companion; these are discussed in the last chapter.

iii) Rotational Interactions.

It is also possible for the advance of periastron to be caused in part by rotational distortion of the companion. This effect is non-negligible if the companion is a rotating helium star or rapidly rotating white dwarf (P < 100 s).

The rotational advance $\dot{\omega}_{rot}$ for a uniformly rotating companion in the case where the spin angular momentum is much less than the orbital angular momentum is (S & B, eq. 3.14)

$$\dot{\omega}_{rot} = 0.84\, \alpha_6 \left(\frac{M_T}{M_\odot}\right)^{-2/3} \left(1 - \tfrac{3}{2} \sin^2\theta_t\right) \qquad \text{(IV-12)}$$

where θ_t is the angle between the companion's spin axis and the normal to the plane of the orbit, and

$$\alpha_6 = \frac{2}{3} \times 10^6 \left(\frac{k_2 R_c^5 \omega_c^2}{G M_c}\right) \ km^2 \qquad \text{(IV-13)}$$

with ω_c being the angular frequency of the companion. There are also observable consequences for this case that will be discussed later.

§4. Gravitational Radiation

There is another General Relativistic effect that may be detectable in the binary system, the orbital spin up due to the loss of energy through gravitational radiation (Esposito and Harrison 1975, Wagoner 1975). The energy loss to the

binary is (Peters and Mathews 1963, Peters 1964)

$$\frac{dE}{dt} = -\frac{32}{5}\frac{G^4 M_p^2 M_c^2 M_T}{a^5 c^5} F(e) \qquad \text{(IV-14)}$$

where $F(e) = (1-e^2)^{-7/2}\left(1+\frac{73}{24}e^2+\frac{37}{96}e^4\right) \approx 11.858$

Using Kepler's law and the observed values of the orbital elements, the equation may be put into the form (Wagoner 1975)

$$\frac{dP_b}{dt} = -8.51 \times 10^{-13} \frac{(M_T/M_\odot)^{4/3}}{\sin i}\left(1 - .507 \frac{(M_T/M_\odot)^{-4/3}}{\sin i}\right) \qquad \text{(IV-15)}$$

and the corresponding timescale for orbital period change is

$$\tau_{GR} \equiv \frac{P_b}{|\dot{P}_b|} \approx 3.8 \times 10^8 \left(\frac{M_p M_c}{(1.42 M_\odot)^2}\right) \text{yr}$$

The predicted decrease in period is relatively insensitive to inclination angle for pulsar masses of $1M_\odot$ or greater. As this is the mass range indicated by the best fit for γ, a reasonably specific prediction of $\dot{P}_b \sim -2.3 \times 10^{-12}$ ss^{-1} can already be made, in good agreement with the detected value of $(-2.0\pm1.0) \times 10^{-12}$ ss^{-1}. It may require several more years of observations to determine the period change to 10% accuracy. By that time, the individual masses and the inclination angle should be well-known, and a more definite prediction possible.

Before a detected $\dot{P}_b$ can be taken as a reliable test of General Relativity, several competing effects must first be shown to be negligible. The following paragraphs discuss briefly the more important of these effects.

i) Tidal Dissipation.

It is possible for the binary system to dissipate orbital energy in tidal interactions between the pulsar and the companion. This dissipation is only significant for a white dwarf or helium star companion. S & B have derived the characteristic timescale τ_t for the tidal interaction.

For a $1.0M_\odot$ helium star, we have (S & B equation 3.20)

$$\tau_t \approx \frac{4\times10^{10}}{\langle\mu\rangle_{13}} \text{ yr} \qquad \text{(IV-16)}$$

where $\langle\mu\rangle_{13}$ is the mean viscosity in 10^{13} gm cm^{-1} s^{-1}. For tidal dissipation to be a significant factor, we require $\langle\mu\rangle_{13} \sim 1$. This is obtained in the presence of a turbulent atmosphere (Balbus and Brecher 1976) or tidally driven shear (Press, Wiita, and Smarr 1975).

For a white dwarf companion, the smaller size and higher density require an even stronger viscous coupling.

$$\tau_t \approx \frac{10^{16}}{\langle\mu\rangle_{13}} \text{ yr} \qquad \text{(IV-17)}$$

It has been suggested that magnetic viscosity in a white dwarf could make $\langle\mu\rangle_{13} \sim 10^5$ or greater, and the timescales for the period to change $\lesssim 3 \times 10^9$ yr (Wagoner 1976). It appears unlikely that the tidal dissipation in the system would be comparable to gravitational radiation losses.

ii) Mass Loss.

As the pulsar spins down, it will lose mass in the form of relativistic particles and electromagnetic radiation.

This mass loss will cause a rate of change of the orbital period. The associated timescale τ_ℓ is

$$\tau_\ell = \left|\frac{2M_T}{\dot{M}}\right| \qquad \text{(IV-18)}$$

where $\dot{M}$ is the combined mass loss rate for the system.

The loss rate from the pulsar can be calculated from its spin down rate. If the pulsar moment of inertia is $I = 10^{45} I_{45}$ g cm^2, then we obtain

$$\dot{M}_P \approx 3\times10^{11} I_{45} \text{ g s}^{-1} \qquad \text{(IV-19)}$$

and the corresponding timescale is

$$\tau_\ell \approx 2\times10^{14} \text{ yr} \qquad \text{(IV-20)}$$

For mass loss from the companion to appreciably affect the orbital elements, we require $\dot{M}_c \gtrsim 10^{-8} M_\odot$ yr^{-1}. A young, rapidly rotating neutron star such as the Crab pulsar could effect a period change on a timescale of $\sim 2 \times 10^8$ yr. However, the associated remnant should have been detected. Only in an extreme case could the helium star support a mass loss of this magnitude. This mass loss should be easily detectable as a variable dispersion measure as described in section 3 of chapter III. We conclude that mass loss cannot significantly change the orbital period.

iii) Motion of the Barycenter.

If the binary barycenter is undergoing acceleration or has an extremely high translational velocity (Brumberg et al. 1975, Blandford and Teukolsky 1975, S & B) there could be a

significant contribution to the period change. However, the pulsar period derivative would be similarly affected. Except in the case of a near cancellation of two large but nearly equal effects, we can set a lower limit to the timescale of any of these effects with the pulsar spin down rate.

$$\tau_a > \tau_{psr} \approx 2 \times 10^8 \text{yr} \qquad \text{(IV-21)}$$

One possible source of acceleration of the system barycenter with respect to the solar system is the galactic rotation. Shapiro and Terzian (1976) have shown that the timescale for period change due to the galactic rotation law τ_g is

$$\tau_g \sim 10^{11} \text{yr} \qquad \text{(IV-22)}$$

and should have no measurable influence.

§5. Precession of the Pulsar

If the spin axis of the pulsar is at a non-zero angle θ_t from the normal to the orbital plane of the system, the pulsar will undergo precession. The dominant effect is de Sitter geodetic precession. The first comprehensive study of the details of precession was performed by Hari Dass and Radhakrishnan (1975). They have determined that the time averaged precession Ω of the axis of rotation about the orbital normal is given by

$$\Omega = \frac{3}{2} \frac{G^{3/2}}{c^2} M_c \frac{(4M_p + 3M_c)}{3M_T^{1/2}} \frac{1-e^2}{a} \text{ rad orbit}^{-1} \qquad \text{(IV-23)}$$

or about 1.2 degrees per year for the best current value of γ, assuming that General Relativity provides an adequate description of the system.

The precession of the pulsar may give observers an opportunity to obtain two dimensional information about various properties of the pulsar emission beam. As the pulsar precesses, the line of sight from the solar system will make a different series of cuts through the pulsar beam. For the first time, a two dimensional map may be obtained of the pulsar emission region with information concerning pulse shape and polarization, and the flux and spectrum. In pencil beam models if precession causes the pulsar beam to move out of the line of sight the pulsar may disappear altogether after 10 or so years.

The pulsar precession may also allow testing of the light cylinder model. If the emission from the pulsar is a fan beam rather than a pencil beam, the pulsar will not disappear, though the flux polarization and pulse shape may still be affected.

Hari Dass and Radhakrishnan discuss an additonal possibility. In the event that we are precessing into the pulsar beam, we may be able to observe perfect alignment of the line of sight with the radiation core axis. A measurement of the intrinsic polarization angle at this time would yield the position angle of the projected rotational axis on the sky in a model dependent way. The position angle information

could be used as a test of the asymmetric radiation model of Harrison and Tademaru (1976).

It is only now becoming feasible to measure the polarization of the mean pulse profile to the accuracy required for these tests. The Swept L.O. system (McCulloch, Taylor, and Weisberg 1978) will permit sampling of the 4 Stokes parameters at sampling intervals of around 100 - 200 μs with this system; meaningful measurements of the sweep of position angle across the mean pulse profile can be made. A trial run of the Swept L.O. system has provided a baseline of almost a year between the high quality profile of 1977 July - August and the 1978 June Swept L.O. data. The mean pulse profile from 1978 June shows a tantalizing shift of the middle peak relative to the older pulse profile, as can be seen in Figure IV-2. This change, in addition to the flux variations described in chapter III section 1, suggests that the precession of the pulsar has been observed. Acquisition of additional high quality data in the near future may confirm this suspicion. The timescale of the changes is in good agreement with the range of values predicted by Hari Dass and Radhakrishnan.

§6. Tests of Gravitational Theories

The final section of this chapter consists of a summary of the several tests of General Relativity and of alternative theories of gravitation afforded by the binary system. Some of these tests require precise knowledge of the individual

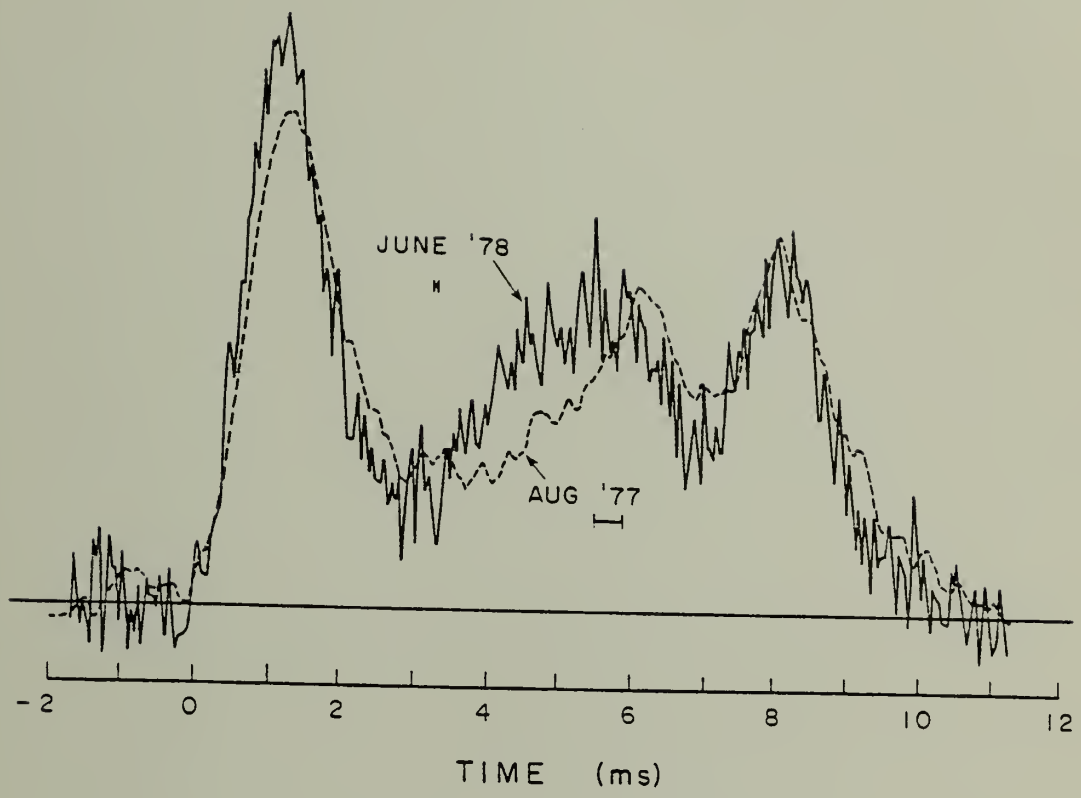

Figure IV-2. A superposition of two 430 MHz pulse profiles. The solid line indicates the 1978 June Swept L.O. profile. The dashed line indicates the 1977 July - August profile taken with the standard observing setup. The time resolution is indicated by the bar beneath the observation dates.

masses of the components of the system. However, several tests provide limits of alternate theories, given only observables well established at the present time.

Comparison between alternative metric theories of gravity is best accomplished (in the weak field limit) with the use of the Parametrized Post-Newtonian (PPN) formalism. With the formalism, the theories differ from each other only in the values of 10 dimensionless parameters. Any gravitational experiment may then be regarded as a measurement of one or more of these values, and in this fashion provides a test of the alternative theories. Descriptions and development of the PNN formalism is available in Weinberg (1972) and Misner et al. (1973). Included in Appendix III is a table of current viable metric theories and their associated PPN parametric values.

i) Gravitational Radiation.

Section 4 of this chapter discussed the possibility of indirectly detecting gravitational radiation in the binary system by observing a spin up of the orbital period with an associated timescale of $\tau_{GR} \approx 3.8 \times 10^8$ yr. Most alternative theories of gravity predict the existence of dipole radiation. The dipole radiation would carry away significantly more energy than the quadrupole radiation associated with General Relativity. For instance, the Brans-Dicke Theory (1961) has a dipole radiation timescale $\tau_{BD} \approx 10^7$ yr (Eardley 1975). The current observed $\dot{P}_B$ is consistent with General Relativity,

and can be used to set very stringent limits on alternative theories. Dipole radiation disappears for equal mass components, so the limit is transformed into a limit on 1 - X, the difference between 1 and the mass ratio. The dipole radiation parameter K_D is listed in Table IV-1, as well as the limit on 1 - X, for the theories discussed by Will and Eardley (1977) and Will (1977). For these calculations, the observed value of $\dot{P}_B$ of -2×10^{-12} was used. Final tests must await the determination of the mass ratio, however, the theories of Ni, Lightman-Lee, and Rosen already require the masses of the two components to be within 1%. The calculation assumes that the pulsar and the companion behave dynamically as point masses.

Recently Rosen (1977) has suggested that gravitational radiation may not carry energy away from a source. The suggestion is based upon the time-symmetry of the field equations for gravitational radiation. For General Relativity, as well as the other viable metric theories, the solutions to the field equations would also be symmetric, with the consequence that the binary system will not lose or gain energy by emitting gravitational radiation. The detection of $\dot{P}_B$, if in fact it is due to energy loss from gravitational radiation, indicates that the time-symmetry must must somehow be destroyed and only positive energy from the retarded potential is carried away from the source.

Theory (reference)	K_D	Max $\|1 - X\|$	
Ni (1973)	$-\frac{400}{3}$	0.004	
Lightman and Lee (1973)	$-\frac{125}{3}$	0.008	
Rosen (1973)	$-\frac{20}{3}$	0.020	
Brans and Dicke (1961)	$\frac{2}{2 + \omega}$	0.102	Note 1.
General Relativity	0		Note 2.

Note 1. Calculation assumes a scalar coupling constant $\omega = 6$.

Note 2. Dipole radiation is forbidden in General Relativity. Because of the large uncertainty in the determination of $\dot{P}_b$, the quadrupole radiation provides no useful limits on the mass range.

Table IV-1. Permitted range of the mass ratio for theories of gravitation.

ii) Limits to PPN parameter ζ_2.

In some non-conservative metric theories of gravity, the center of mass of a binary system may "self-accelerate" in the direction of the system's periastron. The violation of momentum conservation is not present in General Relativity or in any semi-conservative theory of gravity, and there are few current viable theories with $\zeta_2 \neq 0$ (Will 1976). However, ζ_2 is also a measure of the contribution of self-gravitational energy to the relativistic "active" mass of an object and is sensitive to the value of ζ_2. Tests to date have produced only the weak limit of $|\zeta_2| < 100$ (Shapiro and Teukolsky 1976).

For the binary pulsar, the contribution to the pulsar period derivative $\dot{P}$ would be (Will 1976)

$$\dot{P} \approx -4 \times 10^{-16} \zeta_2 \frac{X(1-X)}{(1+X)^2} M_T^{2/3} T \qquad \text{(IV-24)}$$

where X is the mass ratio M_p/M_c and T is the time span in years from 1974 September. In the case of identical masses, the acceleration is zero, so a determination of the masses will be prerequisite to a definitive test. However, for $(1 - X) > .1$, we have $|\zeta_2| < .036$. After an adequate determination of X, $\dot{P}$ will provide the first good limit on ζ_2.

iii) Anisotropic Gravity.

In the event that anisotropic post-Newtonian metric potentials exist, celestial bodies would have anisotropic inertial and/or gravitational masses (Nordtvedt 1975). The

current value of the periastron advance of the binary pulsar has been used by Nordtvedt to place an upper limit on the magnitude of such an effect. If less than .5° yr^{-1} of the periastron advance is due to the anisotropy, the magnitude of the anisotropy matrices is limited to be less than 10^{-4} or 10^{-5}. A fit to the data with an added parameter $\dot{\omega}_N$ may be justifiable after approximately 10 years of observations to place an even stronger limit to the anisotropy. At that time a several years' periodicity in the anisotropic precession would allow separation of that term from classical or relativistic precession terms.

iv) Advance of Periastron as a Test of Alternative Gravitational Theories.

If an independent, non-relativistic method can be used to determine the inclination of the system, the periastron advance could be made into a test of General Relativity and other viable theories. The full PPN form of the periastron advance is

$$\dot{\omega}_{PPN} = 2.11\left(\frac{M_T}{M_\odot}\right)^{2/3}\left\{\tfrac{1}{3}(2+2\gamma-\beta)+\tfrac{1}{6}(2\alpha_1-\alpha_2+\alpha_3+2\zeta_2)\frac{X}{(1+X)^2}\right\} \qquad \text{(IV-25)}$$

For General Relativity, $\{\gamma = \beta = 1,\ \alpha_i = \zeta_2 = 0\}$. This could be used to test ζ_2, as solar system limits on the other PPN parameters are already fairly strong.

A non-relativistic determination of the inclination angle is required. Measurements determined from aberration effects and polarimetry position angle sweep have been sug-

gested. Any relativistic determination of the inclination (e.g. with the $O(v/c)^3$ terms) may also be contaminated by different PPN values in the fit, and would not be suitably independent. Needless to say, all other sources of periastron advance, such as rotational or tidal effects, must be thoroughly understood. For these reasons, it is not likely that the relativistic advance will prove to be a decisive test of gravitational theories.

v) Precession of the Pulsar Spin Axis.

The pulsar precession described in section 5 of this chapter could be viewed as a test of the PPN parameters of the various theories. The values derived by Hari Dass and Radhakrishnan assume that General Relativity is the proper description of gravitation. The full PPN precession $\underset{\sim}{\Omega}_{PPN}$ is (Will 1978)

$$\underset{\sim}{\Omega}_{PPN} = \underset{\sim}{\Omega}' \times \underset{\sim}{n}$$

$$\underset{\sim}{\Omega}' = \frac{3\pi}{P_b}\left\{\frac{M_c^2}{M_T a(1-e^2)}\right\}\left\{\frac{1}{3}(2\gamma+1) + \frac{2}{3}\left(\gamma+1+\frac{\alpha_1}{4}\right)\frac{M_p}{M_c}\right\}\underset{\sim}{n}_0 \qquad \text{(IV-26)}$$

where γ and α_1 are PPN parameters, $\underset{\sim}{n}$ is the unit vector parallel to the pulsar's spin axis, and $\underset{\sim}{n}_0$ is a unit vector normal to the orbital plane. For general relativity, we have $\gamma = 1$, $\alpha_1 = 0$. The major problem using precession as a relativistic test rests with determining observationally the magnitude of the precession from changes in pulse shape or position angle sweep curves. Of course, if one is willing to wait ~300 yrs until the pulsar precesses back into view, an accurate test indeed would ensue! The orbital and individual

mass elements should be very well-known by then!

C H A P T E R V

CONCLUSIONS

§1. Introduction

The final chapter contains a summary of the salient points and accomplishments of this dissertation. Because observations of the pulsar are an on-going project, there is also included a brief section describing the Swept L.O. observing system and anticipating results that may be obtained in the next few years. This chapter also houses a summary of the several evolutionary scenarios that have been proposed for the binary system, and a section devoted to tests concerning the nature of the companion. In sequential order, the chapter consists of: evolutionary scenarios (section two), the observational tests (section three), the Swept L.O. system (section four), and the summary in section five.

§2. Evolutionary History

One possible approach to determining the nature of the companion is through the development of evolutionary histories of the system. This technique cannot be used to conclusively rule out any companion type, but arguments can be made to the effect that a neutron star companion is the most likely. Schemes have been devised to also produce a black hole, white dwarf, and helium star companion. The different

scenarios are divided into two classes. The first class, referred to by S & B as high mass, consists of those pictures where the total final mass is $2.84M_{\odot}$. The low mass category is populated by systems where the companion is either a rapidly rotating white dwarf (RRWD) or a helium star. In these systems, the classical effects contribute significantly to the advance of periastron, and the total mass of the system is less than $2.84M_{\odot}$.

Neutron Star Mass Limits

Before discussing the binary system history, a digression is necessary. Because an appreciable portion of the periastron advance is caused by classical effects, the low mass systems involve light neutron stars. In particular, the maximum neutron star mass permitted for a neutron star - helium star system is $\sim.6M_{\odot}$. Systems with RRWDs have the full range of permitted neutron star masses. However, neutron stars with masses above $\sim 1M_{\odot}$ are found in systems where the companion rotates extremely rapidly. The required rotation rate of a $.7M_{\odot}$ companion to a $1M_{\odot}$ neutron star is within perhaps 10 seconds of its centrifugal break up limit of about 20 seconds. So low mass neutron stars are once again favored.

There is some observational and theoretical input to this question. The masses of neutron stars in X-ray binary systems are all observed to have masses larger than $.6M_{\odot}$ (M & T, p. 82, Table 5-1) and in the case of Vela X-1,

larger than $1.6M_{\odot}$ (van Paradijs et al. 1976). As these objects are assumed to be progenitors to the binary pulsar system in many evolutionary scenarios, a weak case can be made favoring the heavier system. Theoretically, permitted neutron star masses range from .1 (Pandharipande and Smith 1975) to some as yet undetermined upper limit of around 2 or $3M_{\odot}$. Barring core fragmentation it is a bit difficult to understand the formation of very light neutron stars ($M_{NS} \lesssim .6M_{\odot}$). A supernova is triggered by a pre-supernova core which exceeds $\sim 1.4M_{\odot}$ and implodes. It would be rather surprising if so tightly bound an object could lose much matter in the ensuing explosion. Once again massive neutron stars seem to be favored.

i) Neutron Star Companion.

The following scenario has been constructed from papers by Flannery and van den Heuvel (1975), Webbink (1975b), S & B, and Sutantyo (1977) and references therein. Consider the following sequence of events. The binary system initially consists of a $16M_{\odot}$ primary and a $4M_{\odot}$ secondary. The $16M_{\odot}$ star evolves towards the red giant phase and overflows its Roche limit. After a period of mass exchange, the system consists of a $4M_{\odot}$ helium star and a $16M_{\odot}$ main sequence star. The helium star evolves until continued nucleosynthesis pushes the core over the Chandrasekhar limit and triggers a supernova. The system then enters an X-ray binary stage (van den Heuvel and Heise 1972). The secondary enters its

red giant phase and begins to dump matter back onto the neutron star primary. Most likely the mass loss will exceed by many orders of magnitude the accretion onto the neutron star, and most of the mass will be lost to the system. The orbital separation between the components will diminish. The result will be a ~$4M_\odot$ helium star and the ~$1.4M_\odot$ neutron star.

There is an alternative method by which the close binary system can be produced. If the mass loss from the $16M_\odot$ secondary is sufficiently great, the secondary and the neutron star can be surrounded by a common envelope, quenching the X-ray binary and forming a double core star (Webbink 1975a, Paczynski 1976). The friction of the envelope on the neutron star is a very efficient means of converting orbital angular momentum into spin angular momentum of the envelope. When the orbital radius reaches approximately twice the radius of the $4M_\odot$ He core of the secondary, the frictional luminosity becomes so great that the envelope is completely driven off and a $4M_\odot$ helium star in a $1R_\odot$ orbit with the neutron star result. In either case, the helium star then continues nucleosynthesis until it exceeds its CHandrasekhar limit and forms a second neutron star of about $1.4M_\odot$.

Either of the histories have the great advantage of being able to relate two seemingly disparate facts. The pulsar has the second shortest period known, yet its timing age is extremely long. This is very unusual, because short period pulsars usually have relatively small timing ages. The

magnetic field strength associated with the timing age of PSR 1913+16 for an assumed mass of ~$1.4M_{\odot}$ is ~10^{11} gauss, about an order of magnitude less than the canonical value. If the observed pulsar is the first neutron star formed, the low magnetic field can be explained as the result of the X-ray binary phase (S & B). Additionally, Davidson and Ostriker (1973) have derived equilibrium periods for neutron stars in X-ray binary systems and S & B find that using their equations and a field strength of 10^{11} gauss, the equilibrium period is about 60 ms. The small spin down rate would change the period insignificantly over 10^{7} years.

Several comments are in order concerning the second supernova. If the supernova is considered to be an instantaneous symmetric explosion which caused no mass loss to the companion, the pre-supernova values of the masses, and semi-major axis can be determined from the current values of M_p, M_c, e and a_1. The initial pre-supernova mass is $3.17M_{\odot}$ for a $1.4M_{\odot}$ neutron star companion (see Table 1 of S & B). If there were an asymmetry of ~.1% then a $4M_{\odot}$ is allowable. The papers of Flannery and van den Heuvel (1975) and Sutantyo (1977) contain extensive calculations of the kick velocities and angles required to keep the binary system bound.

There is another process that may have played an important role in the evolution of the high mass system. The acceleration due to asymmetric radiation (Harrison and Tademaru 1975, Tademaru 1976) provides a mechanism whereby the large observed eccentricity may be produced. In the model it is

shown that a rotating dipole magnetic field offset from the spin axis radiates asymmetrically in a direction parallel to the spin axis. The force exerted on the pulsar can be quite important immediately after neutron star formation. If the system is not disrupted by the supernova or the radiation force, the system will tend to align itself so that the asymmetric force (and hence the spin axis) is in the orbital plane and is perpendicular to the line of apsidies. The eccentricity is changed in a fashion dependent upon the initial conditions. Though precession of a pulsar will have long since destroyed the alignment with respect to the line of apsidies, the final configuration may be such that both the pulsar and the companion have their spin axes in the orbital plane. This prediction may constitute a test of the theory, and has consequences for the observational tests of the next section.

ii) Black Hole Model.

The upper mass limit to a neutron star is not well established, and if the neutron star formed during the first supernova event is able to accept sufficient mass during the X-ray or double core phase, a black hole may be produced. The black hole would be observationally difficult to distinguish from another neutron star.

iii) White Dwarf.

S & B develop an evolutionary scenario appropriate for the formation of a high mass white dwarf companion. The

initial system consists of an $8M_\odot$ primary and a $6M_\odot$ secondary. The primary evolves as before to the point where it overflows its Roche lobe. If both angular momentum and total mass are conserved, the end result is a $1.3M_\odot$ carbon - oxygen (C - O) white dwarf ~25 AU from the $12.7M_\odot$ star. If the system goes through a double core stage when the secondary overflows its Roche lobe, the white dwarf will spiral in towards the core (which looks like a $3.5M_\odot$ or $4M_\odot$ helium star) and most of the mass and angular momentum of the system will be lost. The result is a pre-supernova configuration with a white dwarf companion. It should be noted that the white dwarf can be differentially rotating (Ostriker and Bodenheimer 1968). Stable differentially rotating white dwarfs exist to $\sim 2M_\odot$, so all inclination angles are permitted for this system.

Next we consider evolutionary sequences that lead to a low mass system, where a significant portion of the observed periastron advance is due to classical effects.

iv) Helium Star Companion.

S & B reconsider the evolution of the white dwarf described above. If there is severe mass and angular momentum loss as the $8M_\odot$ primary overflows its Roche lobe, then its $1.3M_\odot$ white dwarf core will spiral inward towards the $6M_\odot$ star, and most of the $8M_\odot$ envelope will be lost. If the white dwarf is as close as 50 $R_\odot$ from the $6M_\odot$ star, then the system will form a double core star before helium is ignited

in the core. The pre-supernova configuration would then be a $1.3M_{\odot}$ white dwarf and a $.6M_{\odot}$ helium core. One problem with this scenario is that the orbital radius resulting from the double core stage seems to be too small by a factor of about $3(2R_{He} \approx .25R_{\odot})$.

The helium star should still possess a small hydrogen envelope, which would in time expand and overflow the Roche lobe. Accretion onto the white dwarf would then push that star over the Chandrasekhar limit to trigger the supernova. The total mass of the system would then be $\sim 1.2M_{\odot}$.

v) White Dwarf Companion.

S & B append the helium star evolution considered in iv) with a brief description of how a RRWD could be found. The helium star may have had time since the supernova to evolve into a white dwarf. If it was co-rotating with the first white dwarf and conserved angular momentum as it contracted, then the spin would be the value required to cause the classical periastron advance needed in that system.

Van Horn et al. (1975) have proposed a different scheme to produce a white dwarf companion. The initial masses are taken to be $2M_{\odot}$ and $1M_{\odot}$. The primary undergoes mass loss to the secondary and then, as a $\sim 1.3M_{\odot}$ white dwarf, accretes mass back from the now expanding secondary. The separation between the two stars diminishes at this point, proposed mechanisms being double core stars, tidal or gravitational dissipation. Eventually the Chandrasekhar limit is exceeded

and the ensuing supernova blasts most of the remaining hydrogen from the system. The secondary then becomes a white dwarf of less than ~$1M_{\odot}$ and in the final contraction may spin up to account for the observed periastron advance.

iv) Discussion.

The most probable companion from an evolutionary point of view seems to be another neutron star. Such a system can be followed through accretion, X-ray binary and double core stages with a good deal of confidence. The agreement between the observed short period and equilibrium period predicted by the accretion lends a considerable amount of support to a two neutron star system. However, other evolutionary scenarios can be constructed, leading to black hole, white dwarf, and helium star companions. Though there are problems with evolutionary timescales being too long or final separations too small, it is nonetheless impossible to rule out any of the proposed companions on evolutionary grounds.

§3. Inquiries into the Nature of the Companion

In this section, three investigations into possible observable consequences of an RRWD or helium star companion are presented. The first two involve placing limits on the permitted tilt angle of the companion's spin axis with respect to the orbital plane. The third is a brief discussion of the reported detection of a star at the timing

position of the pulsar (Kristian et al. 1978).

i) White Dwarf Companion.

S & B have developed a test whereby an RRWD companion could be detected observationally. For a given tilt angle θ_t between the RRWD spin axis and the orbital angular momentum vector, they derive a relationship between the classical periastron advance and a change in the inclination angle of the system (section IIIb). The off axis rotation results in a component of the distortion out of the orbital plane and the orbit undergoes an oscillation about a fixed angle with respect to the plane of the sky. The rotational contribution $\dot{\omega}_{rot}$ to the advance is

$$\dot{\omega}_{rot} = 0.84\,\alpha_6 \left(\frac{M_T}{M_\odot}\right)^{-2/3} \text{deg yr}^{-1} \qquad \text{(IV-11)}$$

For small θ_t (shown below to be appropriate), the change in inclination angle is found to be $d/dt(i) \sim \theta\dot{\omega}_{rot}$. Using the observed value $\dot{\omega}$ and an upper limit of $d/dt(i)$ equal to the formal error of that term, we can derive a very stringent limit of $\theta_t \lesssim .014°$. An alignment of that precision in the system is highly unlikely. The asymmetric radiation force or a slightly asymmetric supernova would suffice to tilt the orbital plane of the system. Dissipative forces cannot be very strong in the system, since the observed eccentricity is still very large. Any original tilt should still be present.

There are a number of comments that must be made. The

first involves assumptions made in the derivation. Equation IV-11 is strictly true only for rigid body rotation. If the white dwarf behaves like a fluid or executes some form of uniform rotation, the spin momentum will perform much the same motion, possibly with the addition of nutation. Secondly, special angles $\{\theta_t = \sin^{-1}(\sqrt{3/2})$ and $\pi/2\}$ must be excluded. The only problem occurs with $\theta_t = \pi/2$. In the event that the asymmetric radiation force dominated the early history of the binary system, and the pre-supernova components had their spin and orbital axes aligned (the most probable case) then we may expect the spin axes of the two stars to be found in the plane of the orbit, i.e. $\theta_t = \pi/2$ (Harrison and Tademaru 1976). For this case, periastron advance can occur with no corresponding change in the orbital inclination, and the limit derived above is invalid.

The third possibility is that the least squares program might absorb the change in inclination angle in another parameter. For an RRWD - neutron star system, the anticipated oscillatory period of the orbital inclination is of order a few hundred days. Barring an improbable coincidence of an oscillation of about 365 days, the change in inclination angle should show up in the error of the $a_1 \sin i$ term.

ii) Helium Star Companion.

If the helium star has a rotational period of 2 hours or less, rotational distortions will approach the magnitude

of the tidal distortions (Roberts et al. 1976) and the change in the orbital inclination angle would be detectable in the manner described above. Tidal distortions by themselves can have no effect on the inclination angle, as they are raised symmetrically with respect to the orbital plane. However, it is possible for the symmetry to be destroyed by slow rotation. It seems that this effect has not been studied before. An observable change in the orbital inclination angle should again be proportional to the tilt angle θ_t. This phase lag effect is responsible for the increase in the semimajor axis of the earth - moon system. A similar effect may also occur with a helium star companion, detectable as $\dot{P}_b$. The sign of $\dot{P}_b$, as well as the sign of $\dot{\omega}_{lag}$, the change of the longitude of periastron caused by the phase lag, is decided by the specific dynamics of the system. The following is an order of magnitude calculation of the importance of this effect.

Assume that the helium star rotates synchronously ($\Omega_{He} \approx \Omega_{orb} = \Omega$). The rotation term can be neglected. The time that it takes the tidal bulge to dissipate (and hence the degree to which the tidal distortion is carried out of the orbital plane) is roughly the sound travel time t_s through the star

$$t_s \sim (G\rho)^{-1/2} \qquad \text{(V-1)}$$

For a $.5M_\odot$ helium star, $t_s \sim 100$ s. The torque N exerted on the pulsar will be (Jeffreys 1959)

$$N \sim Ma^2\dot{\omega}_{lag} \sim \frac{GM^2R_c^5\langle\rho_c\rangle}{a^5} \sin 2\varepsilon \qquad (V\text{-}2)$$

where $\langle\rho_c\rangle$ is an averaged density of the companion, M and a are typical masses and separations in the system, and ε is the phase lag angle. The precession of periastron due to the phase lag will then be

$$\dot{\omega}_{lag} \sim \frac{MGR_c^2\varepsilon}{a^5} \qquad (V\text{-}3)$$

for small ε. The change in inclination angle should go roughly as $\theta_t\dot{\omega}_{lag}$. For synchronous rotation, $\varepsilon \sim \Omega t \sim .02$. Upon substitution of values we have $\dot{\omega}_{lag} \sim .03$ deg yr^{-1}.

The effect is too small to provide a good limit on θ_t. Detailed calculations would be appropriate in the event that the companion is a helium star, because the effect might be detectable for large θ_t, and could provide information on the orbital tilt angle.

iii) Optical Observations.

Kristian and Westphal (1978) report a detection of an object of magnitude ~22.5 at the timing position of the pulsar. The observation would be a significant one, and might be extremely useful in determining the companion type.

The following discussion will focus on two aspects of the detection. The first is concerned with the chance superposition of a background star at the expected position. The second attempts to use estimates of helium star luminosities, pulsar optical luminosities, and the expected amount of red-

dening to determine if the pulsar or the companion might have been detected.

Chance Superposition

Based on a slight extrapolation of the table of A_m, the number of stars per square degree within the brightness range $m + 1/2 \leftrightarrow m - 1/2$ for galactic latitude 0° (Allen 1973, §117, p. 293), we have that there should be $\sim 10^{5.3} = 2 \times 10^5$ stars deg^{-1}. The chance that a background star may be found within 1 arcsec of the timing position is then roughly equal to the density of stars $arcsec^{-2}$, N, for that magnitude range

$$N \sim \frac{2 \times 10^5}{60^4} \sim .02 \text{ arcsec}^{-2} \qquad \text{(V-4)}$$

We conclude that it is unlikely that a background star would be found at the timing position.

Possible Detection-analysis

There are two possibilities. The detected object could be a helium star companion or faint optical emission from the pulsar, akin to that detected from the Crab pulsar or the Vela pulsar (which has the third shortest period, 89 ms).

Reddening

An attempt to predict the apparent magnitude of an optical object in the binary system will have to allow a correction for interstellar absorption. Davidsen et al. (1975) studied seven stars in the area of the pulsar timing position. They were able to estimate the extinction, color excess, and distance for these stars. They determined a value

of 1.5 ± .3 kpc^{-1}, or atotal of 7 magnitudes of reddening. It is possible that the line of sight may break out of the reddening layer before reaching 5 kpc, and the absorption ~3 - 4 mag.

Helium Star as the Observed Companion

Helium stars have luminosities in the range of 1 - 10^3 $L_\odot$, however the bolometric corrections are large (~-5 mag). The absolute magnitude in the visual band of a 30 $L_\odot$ helium star should be ~6. At 5 kpc with 3.5 magnitudes of extinction, we have an estimated apparent magnitude of 23. We conclude that it is possible for the detected object to be a helium star.

Optical Emission

If the difference in luminosity between the Crab and Vela pulsars is attributable to the longer period of the Vela pulsar, then it can be shown that the optical luminosity must scale as $\sim P^{-12}$. This value is in excellent agreement with the ~5% yr^{-1} decrease of the optical emission of the Crab pulsar reported by Kristian (1978). If the same scaling holds for PSR 1913+16, then the pulsed emission should be a factor of ~1000 less than the Crab pulsar. At 2.5 times the distance we anticipate that the time-averaged pulsed emission should be approximately 11.5 magnitudes fainter than the Crab pulsar emission (m_{CRAB} ~ 16.5), or about 28 mag.

If the optical emission mechanism is incoherent synchrotron radiation, then a scaling of $\sim P^{-10}$ is expected. This

model is not excluded by existing data (M & T). For this scaling law, a visual magnitude of ~27 results. In addition, not all the emission need be pulsed. If only 5% of the optical emission is pulsed, then an apparent visual magnitude of 23.5 would result. This possibility is suggested by the observation of a substantial amount of non-pulsed optical emission from the Vela pulsar (Manchester 1978).

Discussion

It seems that the observed star is most likely the companion star. Under the most favorable of scaling laws and total emission assumptions, the pulsar should have an apparent magnitude of ~23.5, about one magnitude fainter than the detected value. The calculation when based on the observational law yields an apparent time-averaged magnitude of ~28, in good agreement with published limits (Nather et al. 1977). However, this pulsar has had a considerably different evolutionary history than either the Crab or Vela pulsar, and there remains a small chance that the detected object is the pulsar.

§4. Future Developments

Timing observations of the binary pulsar are continuing, and the next scheduled observing session is 1978 October. With this and the next several sessions, it is hoped to achieve a long baseline of high quality timing data. The new observing system is described below.

i) The Swept L.O. System

Attempts to improve the time resolution of binary pulsar timing data must deal with two conflicting needs: the desirability of having small bandwidths to achieve the time resolution and the necessity of having large enough bandwidths to acquire sufficient signal-to-noise. McCulloch and Taylor have devised an observing system whereby the dispersive delay introduced by the interstellar medium is removed before detection and problems with large bandwidths are much less severe. The resulting pulse profile has effectively 43 μs smearing and a corresponding increase in timing accuracy is expected. The predetection dispersion removal is accomplished by tracking the downward frequency sweep of the pulse with a variable local oscillator, offset by a small amount from the observing frequency. In this fashion, the time dependence of the arrivals at different frequencies is removed, and the pulse is observed continuously over a total frequency bandwidth determined by the pulsar period and dispersion measure. The preliminary test of the system in 1978 June had 5 times the bandwidth of previous 430 measurements, and nearly 10 times less dispersive smearing.

ii) Future Studies.

The focus of future observations will continue to be acquisition of timing data. The next few sessions should bring about the firm establishment of the pulsar and companion masses. See Figure V-1 for a plot of the learning curve

Figure V-1. The fractional accuracy to which the values of the four relativistic parameters are known is plotted against the date of the determination. The curves are then drawn by hand. The slopes of these learning curves are the result of complicated interactions between longer time baselines, smaller observational measurement uncertainties, and the application of better fitting techiniques to the data.

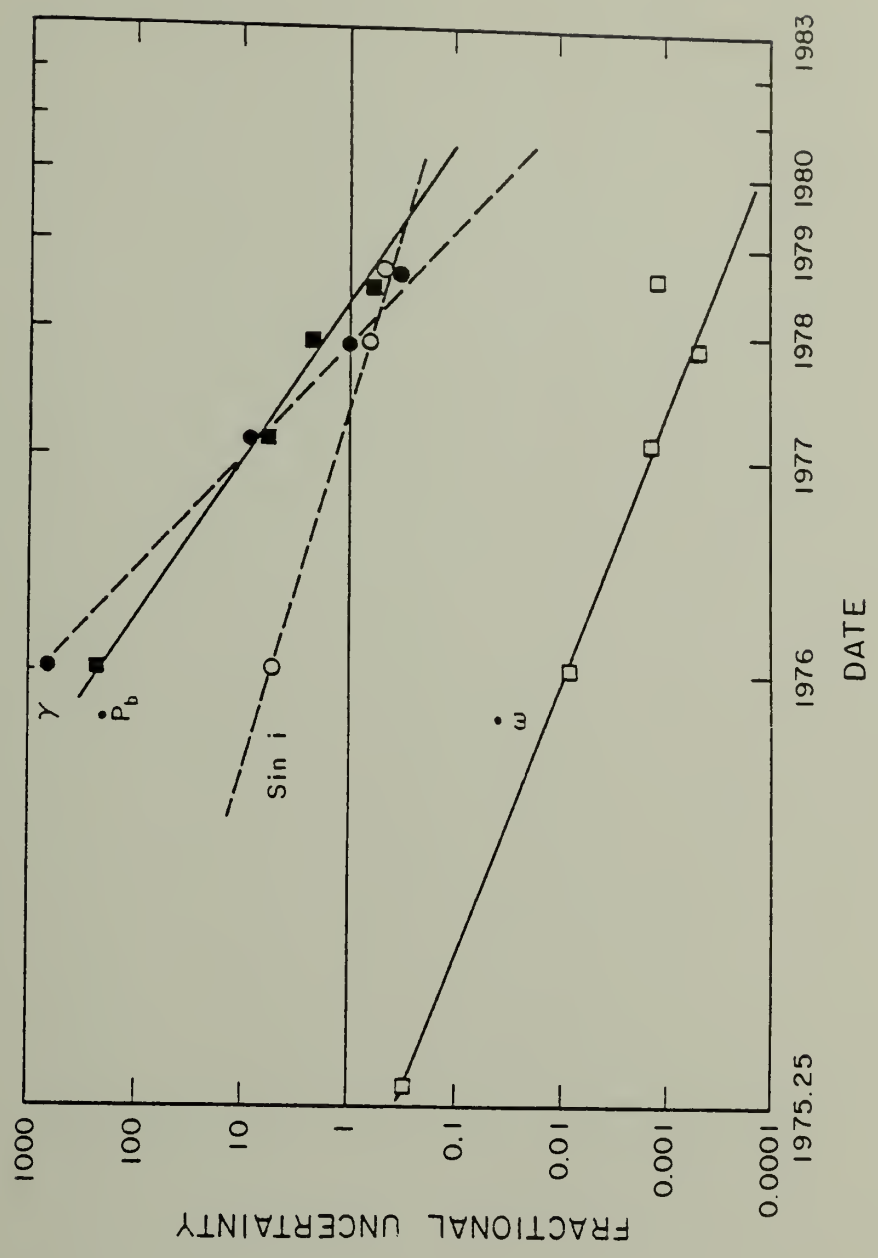
FRACTIONAL UNCERTAINTY
1000
100
10
1
0.1
0.01
0.001
0.0001
1975.25
1976
1977
1978
1979
1980
1983
DATE
γ
$\dot{P}_b$
Sin i
$\dot{\omega}$

for these relativistic effects. The over-determination provided by the $O(v/c)^3$ terms will serve as an all-important check on the assumption that the system behaves dynamically like two point masses. The values of the masses will then allow exact calculation of a number of the relativistic effects and gravitational tests detailed in the last chapter. Chief among these will be specific predictions of gravitational radiation losses for the system in General Relativity and other gravitational theories. The General Relativity prediction can be compared to the $\dot{P}_b$ value derived in the fit. Also, the upper limit to ζ_2 will be established more definitively.

The increased accuracy of the timing data might warrant the inclusion of an additional fit term: λ, the angle between the pulsar spin axis and the orbital angular momentum axis. The determination of the spin axis orientation would come from Galilean aberration effects. The spin axis orientation would serve as an important test of the asymmetric radiation model, as well as aid in the interpretation of polarimetry observations.

An important by-product of the timing observations is the mean pulse shape. The precession of the pulsar is best studied from the pulse shape changes in time, though future observations should include a few flux calibrations to monitor associated flux changes. The calibrations would be rather simple to perform, and could prove invaluable in

studying pulsar radiation patterns.

Additional polarimetry should also receive a high priority. The Swept L.O. system is amenable for use in a 4 × 252 channel mode, and would allow simultaneous acquisition of the 4 independent polarizations necessary to determine the Stokes parameters. The time resolution can be increased by nearly a factor of 10 above that used in the studies reported in this dissertation. Accurate absolute position angle determinations and the mean pulse polarization structure can provide a wealth of emission mechanism information if continuous monitoring is pursued for several years.

§5. Summary

The binary pulsar has proven itself to be a fascinating and extremely valuable object for study. Four years of timing data have allowed a preliminary determination of the system masses, as well as a tentative consistency check from the $O(v/c)^3$ terms and an indication of the presence of orbital spin up due to gravitational radiation. This final section is a heuristic description of the binary system that emerges from research to date.

The timing data strongly suggests that the system is composed of two compact stars of nearly equal mass in an $\sim 1 R_\odot$ mutual orbit inclined to about 45° from the plane of the sky. From evolutionary history arguments, the companion is most likely another neutron star. There is a well

determined advance of the longitude of periastron in the system, most probably due entirely to relativistic gravitational effects. These effects are also to be found in high order terms in the timing data, and future observations will provide a significant increase in the accuracy to which we know the orbital elements and relativistic effects. We wish to emphasize again that all three relativistic effects ($\dot{\omega}$, sin i, and $\dot{P}_b$) are consistent to within the formal errors with each other, with General Relativity, and with a system composed of two point masses with a total mass of $\sim 2.84 M_\odot$. The only serious problem with a wholehearted adoption of this interpretation of the system may be the optical detection. There is some chance that the detected object is the pulsar. If the detected object is the helium star, then the consistency of the three relativistic effects is not expected, though it could be contrived. A resolution of this discrepancy must await additional data.

The observed pulsar is a respectable member of the class. The pulse shape and flux spectrum are typical of pulsars in general, as are the average pulse polarization characteristics. The 430 MHz signal is about 25% linearly polarized, with no detected circular polarization. The companion does not seem to interact in any way with any of these observables. The lack of dispersion measure change with orbital phase sets an upper limit of $\sim 10^5$ electrons cm^{-3} in the vicinity of the pulsar. This limit is not

strong enough to categorically dismiss the possibility of a helium star companion, though the limit on mass loss is more than adequate to rule out the possibility that mass loss could contribute to an orbital spin up of the magnitude of that predicted by General Relativity.

There are two detectable effects of the binary system on the pulsar, both of which are fruitful areas of research. The precession of the pulsar, if confirmed in future observing sessions, provides the first opportunity to look at a two dimensional map of such pulsar quantities as flux, spectrum, pulse shape, and polarization. The other effect is somewhat more speculative, and is related to the evolutionary history of the system. For such a rapid pulse rate, the pulsar spin down rate is extremely small, and interactions with the companion have been proposed to account for this anomaly. In the favored evolutionary scenario, the observed pulsar was born first, and has probably undergone mass exchange in an X-ray binary or double core star phase. The pulsar magnetic field may have been severely attenuated by the accretion, and the pulsar spun up to its present period. Spin ups are commonly observed in X-ray binary systems. The small amount of timing noise evidently present in this source may also be an outcome of the interactive phases in its evolution.

The system as described is a perfect laboratory for relativistic gravitational experiments. These have been described elsewhere and need not be summarized again.

The pulsar and its binary system have been very rewarding to study. Many areas of physics and astronomy are involved, from star counts to gravitational theory. The system is exciting to contemplate and to study, and it presents a wealth of observational and interpretational complexities worthy of many years of effort.

REFERENCES

Aitken, R.G. 1964, The Binary Stars (New York: Dover Publications)

Allen, C.W. 1973, Astrophysical Quantities (3rd ed., London: Athlone Press), p. 293.

Bevington, P.R. 1969, Data Reduction and Error Analysis for the Physical Sciences (New York: McGraw Hill), p. 164

Blandford, R. and Teukolsky, S.A. 1975, Ap.J. Lett., 198,L27.

Boriakoff,V. 1973, "Pulsar Radiofrequency Observations with a Digital Pulse Processor," NAIC #38, National Astronomy and Ionosphere Center, Arecibo, Puerto Rico.

Boynton, P.E., Groth, E.J., Hutchinson, D.P., Naros, G.P., Partridge, R.B., and Wilkinson, D.T. 1972, Ap.J., 175, 217.

Brans, C. and Dicke, R.H. 1961, Phys. Rev., 124, 925.

Brecher, K. 1975, Ap.J. Lett., 195, L113.

Brumberg, V.A., Zel'dovich, Ya.B., Novikov, I.D., and Shakura, N.I. 1975, Sov. Astron. Lett., 1, 2.

Cordes, J.M. and Hankins, T.H. 1977, Ap.J., 218, 484.

Davidsen, A., Margon, B., Leibert, J., Spinrad, H., Middleditch, J., Charan, G., Mason, K.O., and Sanford, P.W. 1975, Ap.J. Lett., 200, 119.

Davidson, K., and Ostriker, J.P. 1973, Ap.J., 179, 585.

Eardley, D.M. 1975, Ap.J. Lett., 196, L59.

Epstein, R. 1977, Ap.J., 216, 92.

Esposito, L.W. and Harrison, E.R. 1975, Ap.J. Lett., 196, L1.

Flannery, B.P. and van den Heuvel, E.P.J. 1975, Astron. Astrophys., 39, 61.

Fowler, L.A., Cordes, J.M., and Taysor, J.H. 1978, Australian J. Phys., in press.

Gold, T. 1968, Nature, 218, 731.

Groth, E.J. 1975, Ap.J. (Suppl.), 29, 431.

Gullahorn, G. 1978, Ph.D. Thesis, Cornell University (unpublished).

Hari-Dass, N.D. and Radhakrishnan, V. 1975, Ap. Lett., 16, 135.

Harrison, E.R. and Tademaru, E. 1975, Ap.J., 201, 447.

Helfand, D.J., Manchester, R.N., and Taylor, J.H. 1975, Ap.J., 198, 661.

Helfand, D.J., Fowler, L.A., and Kuhlman, J. 1977, A.J., 82, 701.

Hewish, A., Bell, S.J., Pilkington, J.D.H., Scott, P.F., and Collins, R.A. 1968, Nature, 217, 709.

Hulse, R.A. and Taylor, J.H. 1974, Ap.J. Lett., 191, L59.

Hulse, R.A. and Taylor, J.H. 1975a, Ap.J. Lett., 195, L51.

Hulse, R.A. and Taylor, J.H. 1975b, Ap.J. Lett., 195, L55.

Jeffreys, H. 1959, The Earth (London: Cambridge University Press), p. 230.

Komesaroff, M.M. 1970, Nature, 225, 612.

Kopal, Z. 1959, Close Binary Systems (London: Chapman and Hall).

Kristian, J. 1978, paper presented at June AAS meeting, Madison, Wisconsin.

Kristian, J. and Westphal, J.A. 1978, IAU Circ., No. 3242.

Lightman, A.P. and Lee, D.L. 1973, Phys. Rev. D, 8, 3293.

Lyne, A.G. and Ritchings, R.T. 1977, Nature, 268, 606.

Manchester, R.N. 1978, private communication.

Manchester, R.N. and Peters, W.L. 1972, Ap.J., 173, 221.

Manchester, R.N. and Taylor, J.H. 1977, Pulsars (San Francisco: W.H. Freeman).

Manchester, R.N., Taylor, J.H., and Huguenin, G.R. 1975, Ap.J., 196, 83.

Masters, A.R. and Roberts, D.H. 1975, Ap.J. Lett., 195, L107.

McCulloch, P.M., Taylor, J.H., and Weisberg, J.M. 1978, in press.

Misner, C.W., Thorne, K.S., and Wheeler, J.A. 1973, Gravitation (San Francisco: W.H. Freeman).

Nather, R.E., Robinson, E.L., Van Citters, G.W., and Hemenway, P.D. 1977, Ap.J. Lett., 211, L125.

Ni, W.-T. 1973, Phys. Rev. D, 7, 2880.

Nordvedt, K., Jr. 1975, Ap.J., 202, 248.

Ostriker, J.P. and Bodenheimer, P. 1968, Ap.J., 151, 1089.

Pandharipande, V.R., Pines, D., and Smith, R.A. 1976, Ap.J., 208, 550.

Paczynski, B. 1976, in Proc. IAU Sympos. 73, Close Binaries (Dordrecht: Reidel), p. 75.

Peters, P.C. 1964, Phys. Rev., 136, B1224.

Peters, P.C. and Mathews, J. 1963, Phys. Rev., 131, 435.

Radhakrishnan, V. and Cooke, D.J. 1969, Astrophys. Lett., 3, 225.

Rankin, J.M., Campbell, D.B., Spangler, S.R. 1976, "430-MHz Radio Astronomical Polarimetry at Arecibo Observatory," NAIC 46, National Astronomy and Ionosphere Center, Arecibo, Puerto Rico.

Roberts, D.H., Masters, A.R., and Arnett, W.D. 1976, Ap.J., 201, 196.

Rosen, N. 1973, J. Gen. Rel. and Grav., 4, 435.

Rosen, N. 1978, Ap.J., 221, 284.

Sutantyo, W. 1977, preprint.

Shapiro, I.I. and Terzian, Y. 1976, Astron. Astrophys., 52, 115.

Shapiro, I.I. and Teukolsky, S.A. 1976, Ap.J., 203, 697.

Tademaru, E. 1976, Ap.J., 209, 245.

Taylor, J.H. 1975, Ann. N.Y. Acad. Sci., 262, 490.

Taylor, J.H., Hulse, R.A., Fowler, L.A., Gullahorn, G.E., and Rankin, J.M. 1976, Ap.J. Lett., 191, L59.

van den Heuvel, E.P.J. and Heise, J. 1972, Nature Phys. Sci., 239, 67.

Van Horn, H.M., Sofia, S., Savedoff, M.P., Duthie, J.G., and Berg, R.A. 1975, Science, 188, 930.

van Paradijs, J.A., Hammerschlag-Hensberg, G., van den Heuvel, E.P.J., Takens, R.J., Zuiderwijk, E.J., and DeLoore, C. 1976, Nature, 259, 547.

Wagoner, R.V. 1975, Ap.J., 196, L63.

Wagoner, R.V. 1976, Gen. Rel. and Grav., 7, 333.

Wagoner, R.V., and Will, C.M. 1976, Ap.J., 210, 764.

Webbink, R.F. 1975a, Ph.D. Thesis, University of Cambridge, England (unpublished).

Webbink, R.F. 1975b, Astron. Astrophys., 41, 1.

Weinberg, S. 1972, Gravitation and Cosmology (New York: Wiley).

Will, C.M. 1976, Ap.J., 205, 861.

Will, C.M. 1977, Ap.J., 214, 826.

Will, C.M. 1979, Einstein Centenary Volume (London: Cambridge University Press), in press.

Will, C.M. and Eardley, D.M. 1977, Ap.J., 212, L91.

A P P E N D I X I

TIMING EQUATION FOR A PULSAR IN A BINARY SYSTEM

The complete timing equation for the binary pulsar is reproduced below. The basic formalism and rationale is set forth in Manchester and Peters (1972). The derivation of the timing equation through $O(v/c)^2$ was accomplished by Blandford and Teukolsky (1976), and Epstein (1977) derived the timing equation through $O(v/c)^3$. The formula desired is the infinite-frequency barycentric arrival time t_∞ which is the time at which a distant observer will detect the Nth pulse, after correcting for relative motion with respect to the solar system, the gravitational field of the solar system, and the frequency dispersion of the pulse caused by free electrons between the pulsar and the observer. At the pulsar surface, the proper time T_P is given implicitly by an equation similar to (II-1)

$$N = N_0 + \nu T_P + \tfrac{1}{2}\dot{\nu} T_P^2 + \tfrac{1}{6}\ddot{\nu} T_P^3 \tag{A-1}$$

The metric used by Epstein is

$$ds^2 = -\left\{1 - 2U + O\left(\tfrac{v}{c}\right)^4\right\} dt^2 + O\left(\tfrac{v}{c}\right)^3 dx^i dt + \left\{1 + 2U + O\left(\tfrac{v}{c}\right)^4\right\} \delta_{ik}\, dx^i dx^k \tag{A-2}$$

where

$$U(\underline{x},t) = \frac{M_P}{(\underline{x} - \underline{x}_P(t))} + \frac{M_c}{(\underline{x} - \underline{x}_c(t))} \tag{A-3}$$

is the potential.

The pulsar is located at position $(X_1, \pi/2, \phi)$ where $\phi = \pi/2$ is the orbital plane, and ϕ is the true anomaly. The two body solution to the equations of motion was found by Wagoner and Wills (1976).

The eccentric anomaly E is used. The relationship between E and the true anomaly ϕ' at t_∞ is

$$\tan\frac{E}{2} = \left(\frac{1-e}{1+e}\right)^{1/2}\tan\frac{\phi'}{2} \tag{A-4}$$

Then, the correction between proper time on the pulsar and observer's time t_∞, (to within an additive constant) is found in terms of the orbital parameters,

$$\begin{aligned} T_p = {} & t_\infty - \alpha(\cos E - e) - (\beta+\gamma)\sin E \\ & + 2m_2 \ln\left\{1 - e\cos E - \sin i\left[(1-e^2)^{1/2}\sin E\cos\omega + (\cos E - e)\sin\omega\right]\right\} \\ & + \frac{\left[\alpha(\cos E - e) + \beta\sin E\right]}{1 - e\cos E}\left(\left\{\frac{\beta+\gamma}{\mathcal{P}} + \Delta e\right\}\cos E - \frac{\alpha\sin E}{\mathcal{P}} + f\,2\cos E\right. \\ & \left. + \frac{1}{2\mathcal{P}^2(1-e\cos E)}\left\{(\alpha\cos E + \beta\sin E)\left[\alpha(\cos E - e) + \beta\sin E\right]\right.\right. \\ & \left.\left. - (\alpha\sin E - \beta\cos E)\left\{2(\alpha\sin E - \beta\cos E) + \frac{e\sin E}{1-e\cos E}\left[\alpha(\cos E - e) + \beta\sin E\right]\right\}\right\}\right) \end{aligned} \tag{A-5}$$

where

$$\alpha = \chi\sin\omega \qquad \beta = (1-e^2)^{1/2}\chi\cos\omega \qquad \mathcal{P} = \frac{P_b}{2\pi}$$

$$\omega = \omega_0 + \dot{\omega}t \qquad \chi = a_1\sin i$$

As described in section 4 of chapter II, the residuals are calculated using estimates of the parameters of the system. These residuals are obtained by substituting equation A-5 into equation A-1 to obtain a predicted time for the Nth pulse, and subtracting this time from the observed arrival time. Dropping the subscript on t_∞ we have that the residual R(t) is

$$
\begin{aligned}
R(t) = {} & \frac{\delta N_0}{\nu} - t\frac{\delta\nu}{\nu} - t^2\frac{\delta\dot{\nu}}{2\nu} + V\left[\frac{t}{P}\frac{\delta P}{P} + \frac{1}{2}\left(\frac{t}{P}\right)^2\delta\dot{P} - \delta\sigma\right] \\
& + \frac{1}{x}\left[\alpha(\cos E - e) + \beta\sin E\right](\delta x + t\delta\dot{x}) + (1-e^2)^{1/2}\left[\frac{\beta(\cos E - e)}{(1-e^2)} - \alpha\sin E\right](\delta\omega_0 + t\delta\dot{\omega}) \\
& - \left\{\alpha + \left[V + \frac{e\beta}{(1-e^2)}\right]\sin E\right\}(\delta e + t\delta\dot{e}) + \sin E\,\delta\sigma \\
& - \left\{2\left(\frac{\partial m_1}{\partial \sin i}\right)_1 \ln\left[(1-e\cos E)\left(1 - \sin i\frac{W}{x}\right)\right] - \frac{2m_2 W}{x - W\sin i}\right. \\
& + V\left[\left(\frac{\partial g}{\partial \sin i}\right)_1 \sin E + \left(\frac{\partial h}{\partial \sin i}\right)_1 \sin 2E\right] \qquad \text{(A-6)} \\
& \left. + W\left[\left(\frac{\partial \Delta e}{\partial \sin i}\right)_1 \cos E + \left(\frac{\partial f}{\partial \sin i}\right)_1 \cos 2E\right]\right\}\delta\sin i
\end{aligned}
$$

where

$$
V = \frac{\alpha\sin E - \beta\cos E}{1 - e\cos E} \qquad W = \frac{\alpha(\cos E - e) + \beta\sin E}{1 - e\cos E}
$$

Please refer to Epstein (1977) for definitions of undefined terms in equations A-5 and A-6.

The coefficient for each term of the fit is then the coefficient associated with that term in the residual equation. Corrections to the fitted parameters are then calculated in a least squares fit to the residuals. The coefficients are used to compute a matrix having the various moments and cross products of the residuals and coefficients as elements. This matrix is then inverted and corrections found by matrix multiplication of the inverse and the initial set of fitted parameters. A complete description of the least squares fit can be found in Bevington (1969). Similarly, error estimates for each term can be calculated.

A P P E N D I X I I

POLARIMETRY

§1. Stokes Parameters

For polarimetry studies, it is usually convenient to describe the signal in terms of the 4 Stokes parameters I, Q, U, V. If the incoming signal consists of a (time averaged) LHCP electric field V_L and an RHCP electric field V_R, then we have

$I = V_L^2 + V_R^2$	the total intensity
$Q = 2V_L V_R$	one linear polarization
$U = 2V_L V_R$(delayed)	the orthogonal linear polarization
$V = V_L^2 - V_R^2$	the circular polarization
$\psi = 1/2 \tan^{-1}(Q/U)$	the position angle of the linear polarization

where V_R(delayed) is the RHCP of signal delayed by $\pi/2$. The fraction of linear and circular polarization are then:

$$\text{fractional linear} = (Q^2 + U^2)^{1/2} / I$$

$$\text{fractional circular} = V/I$$

§2. Calibrations

For polarimetry, it is critical to know the relative gains of the LHCP and RHCP signals. In order to determine the unknown polarization of a source, this calibration must be performed by observing a source having no circularization.

In addition, a temperature calibration must be run on both circular polarization channels, to finally calibrate the linear channels. In order to accomplish these calibrations, the following telescope pointing and temperature calibration pattern was used:

1°N of source On source 1°S of source Left cal on Right cal on.

At 1415 MHz, 30 second integrations were used at each position. 10 seconds of fast-sampled data were gathered at 430 MHz, and then folded to form a set of calibrations equivalent to those at 1415 MHz.

The source for the 1415 MHz cals was 3C 409, which has circular polarization less than 5% and a flux of 13.04 Jy. The left and right temp cals were 5.82°K and 6.65°K respectively.

The calibration source at 430 MHz was 3C 411 having less than 3% circular polarization and a flux of 8.2 Jy. The left and right temp cals were 169°K and 106°K respectively. We made one additional type of calibration. We have performed the calibrations necessary to determine the absolute position angle of the source in the sky. A calibration dipole of known position angle is observed, so that the relative position angle can be related to a position angle in the sky. In addition, PSR 2020+16 was observed at 430 MHz, as a test and check for the system. The absolute position angle corrections to the quoted position angle has not been found, though all

the data are available. Because of the weakness of the pulsar and lack of polarization at 1415 MHz and the poorness of the sampling at 430, the absolute position angle was judged not important. Any future position angle determinations will surely be made at Arecibo at 430 MHz and any differences in the relative position angles will indicate differences in the absolute position angles.

Faraday Rotation

Although not a calbration *per se*, Faraday rotation could be a possible cause of apparent depolarization of the pulsar. Faraday rotation is the rotation of the position angle of a linearly polarized source at different frequencies caused by the propagation of the radio waves through the interstellar medium in the presence of a component of the magnetic field parallel to the line of sight. If the rotation measure R is known, the Faraday rotation at any frequency ν is

$$\Delta\psi = Rc^2/\nu^2 \qquad \text{(A-7)}$$

where $\Delta\psi$ is the rotation of the position angle between infinite frequency and the observed frequency ν. When observing at low frequencies and large bandpasses, it is possible for the rotation of the position angle across the bandpass to significantly depolarize the source. In this case, the differential rotation $\delta\psi$ across a bandpass of $\delta\nu$ is

$$d\psi = -2Rc^2 \frac{\delta\nu}{\nu^3} \qquad \text{(A-8)}$$

Substituting the maximum rotation measure observed in a pulsar (-614 rad. m^{-2}) for PSR 1641-45 we have that the rotation across the 250 kHz bandpass at 430 MHz is less than 20°, and the effects of depolarization are judged not important. Depolarization is even less important at the higher frequency because of the strong ν^{-3} dependency.

§3. Determination of Stokes Parameters

The information from the 4 channels of the polarimeter takes the final form of "displacements" measured in computer units. These displacements are related to the Stokes parameters in the following equations:

$$
\begin{aligned}
I &= \left(\frac{D_L}{R_L} + \frac{D_R}{R_R}\right) \\
Q &= 2\left\{\frac{D_{L+R} - \alpha_R(D_R/R_R) - \alpha_L(D_L/R_L)}{(\alpha_R\alpha_L)^{1/2}}\right\} \\
U &= 2\left\{\frac{D_{L-jR} - \beta_R(D_R/R_R) - \beta_L(D_L/R_L)}{(\beta_R\beta_L)^{1/2}}\right\} \\
V &= \left(\frac{D_L}{R_L} - \frac{D_R}{R_R}\right)
\end{aligned}
\qquad \text{(A-9)}
$$

The units of the D's are computer units, I, Q, U, V are in flux units, and $R_L R_R \alpha_L \alpha_R \beta_L \beta_R$ are in computer units/flux units (c.u./f.u.). The measurement of the standard source gives R_L and R_R in c.u./f.u. The measurement of the calibration temperature in the left and right channels gives R_L/A_L and

R_R/A_R where A_i is the system gain in the ith polarization, from which the system gains A_L and A_R can be determined. Then the α's and β's are determined by the product of the system gain and the calibration temperature response in the linear polarization channels. The resulting fluxes in I, Q, U, and V are determined by substituting the D's, R's, α's, and β's.

Parallactic Angle Corrections

In an altitude-azimuth telescope such as the Arecibo instrument, the telescope field rotates against a fixed angle in the sky, as the source is tracked across the sky. For PSR 1913+16, the correction is very important near transit, where the azimuth arm swings around nearly 180° as the source passes nearly overhead. The circular polarization and total intensity are not affected. In order to compensate for the rotation, the complex linear polarization vector L = Q + iU is formed. The phase of L is then related to the position angle by equation A-5. The phase is adjusted by the parallactic angle as described in Appendix IV of NAIC report #46, Rankin et al. (1976). After the parallactic corrections have been made, the Stokes parameters for each 5 min integration can be summed directly. In this manner, the plots of Figure III-7 were produced.

A P P E N D I X I I I

PPN FORMALISM

The following description of the parametrized post-Newtonian (PPN) formalism is adapted from Will (1979). The formalism was devised in order to study and classify competing theories of gravity. In the weak field, slow motion, post-Newtonian limit, all metric theories differ from one another only by their predictions for a set of 10 dimensionless parameters. Various relativistic effects can then be cast into forms depending explicitly on these PPN parameters and thereby greatly facilitate comparison between experiment and theory. Table A-1 lists the currently used PPN parameters and the values for the parameters for these types of metric theories: a) General Relativity, b) semi-conservative theories based on conservation of momentum (the invariant action principle), and c) fully conservative theories also having global conservation of angular momentum.

The PPN parameters are small numerical coefficients that occur in front of gravitational potentials obtained in the expansion of the space time metric in any given theory about the "flat-space" Minkowskii metric [diag (-1,1,1,1)]. The various parameters have meanings in terms of these potentials. γ is sensitive to the amount of curvature associated with a unit mass as compared to General Relativity, and β tests the amount on non-linearity in the superposition law in each particular theory. ζ is sensitive to preferred-

Table A-1. The PPN parameters. [1.]

Parameter [2.]	Value in General Relativity	Value in semi-conservative Theories	Value in fully-conservative Theories
γ	1	γ	γ
β	1	β	β
ξ	0	ξ	ξ
α_1	0	α_1	0
α_2	0	α_2	0
α_3	0	0	0
ζ_1	0	0	0
ζ_2	0	0	0
ζ_3	0	0	0
ζ_4	0	0	0

Note 1. Adapted from (Will 1979)

Note 2. The significance of the PPN parameters is explained in the text.

location effects (such as a galaxy-induced anisotropy in the local gravitational constant) and α_1, α_2, α_3 predict preferred frame effects. The final set of PPN parameters, ζ_1, ζ_2, ζ_3, ζ_4 as well as α_3 measure violations of global conservation laws for non-conservative theories.